2012-12

Determination of the pressure equivalent noise signal of vector sensors in a hybrid array

Kok, Chuen Wah

Monterey, California. Naval Postgraduate School

NAVAL POSTGRADUATE SCHOOL

MONTEREY, CALIFORNIA

THESIS

DETERMINATION OF THE PRESSURE EQUIVALENT NOISE SIGNAL OF VECTOR SENSORS IN A HYBRID ARRAY

by

Chuen Wah Kok

December 2012

Thesis Advisor:	Daphne Kapolka
Second Reader:	Kevin B. Smith

Approved for public release; distribution is unlimited

THIS PAGE INTENTIONALLY LEFT BLANK

REPORT DOCUMENTATION PAGE			Form Approved OMB No. 0704-0188
Public reporting burden for this collection of information is estimated to average 1 hour per response, including the time for reviewing instruction, searching existing data sources, gathering and maintaining the data needed, and completing and reviewing the collection of information. Send comments regarding this burden estimate or any other aspect of this collection of information, including suggestions for reducing this burden, to Washington headquarters Services, Directorate for Information Operations and Reports, 1215 Jefferson Davis Highway, Suite 1204, Arlington, VA 22202-4302, and to the Office of Management and Budget, Paperwork Reduction Project (0704-0188) Washington DC 20503.			
1. AGENCY USE ONLY ***(Leave blank)***	**2. REPORT DATE** December 2012	**3. REPORT TYPE AND DATES COVERED** Master's Thesis	
4. TITLE AND SUBTITLE Determination of the Pressure Equivalent Noise Signal of Vector Sensors in a Hybrid Array		**5. FUNDING NUMBERS**	
6. AUTHOR(S) Chuen Wah Kok			
7. PERFORMING ORGANIZATION NAME(S) AND ADDRESS(ES) Naval Postgraduate School Monterey, CA 93943-5000		**8. PERFORMING ORGANIZATION REPORT NUMBER**	
9. SPONSORING /MONITORING AGENCY NAME(S) AND ADDRESS(ES) N/A		**10. SPONSORING/MONITORING AGENCY REPORT NUMBER**	
11. SUPPLEMENTARY NOTES The views expressed in this thesis are those of the author and do not reflect the official policy or position of the Department of Defense or the U.S. Government. IRB Protocol Number: N/A.			
12a. DISTRIBUTION / AVAILABILITY STATEMENT Approved for public release; distribution is unlimited		**12b. DISTRIBUTION CODE** **A**	

13. ABSTRACT

The advent of particle velocity sensors as a viable addition to traditional pressure-based sensors in acoustics has fueled considerable research into the additional capabilities they might bring. Previous thesis work performed at NPS successfully demonstrated a working acoustic beamformer using a hybrid array comprised of a single conventional omnidirectional microphone and two 3D Microflown Ultimate Sound Probes in an anechoic chamber. These Microflown sensors are vector sensors. They have integrated directionality through the inclusion of three orthogonal particle velocity sensors with a microphone. Unfortunately, the signals of the particle velocity sensors obtained outside in a light, gusting wind were unusable due to broadband noise. Since the fundamental limit to detecting quiet targets depends on the noise floor, the aim of this thesis was to perform an in situ measurement of the pressure equivalent noise floor of all sensors in the array and to minimize the wind noise. Noise levels measured in an anechoic chamber were 9–15 dB higher than the levels expected from the sensors alone. The additional noise is attributed to the data acquisition equipment. The use of an ACO WS7 windscreen was shown to be extremely effective in mitigating broadband wind noise.

14. SUBJECT TERMS Particle Velocity, Acoustic Array, Acoustic Vector Sensor, Microflown, Hybrid Array, Directional, Pressure Equivalent Noise Floor.			**15. NUMBER OF PAGES** 91
			16. PRICE CODE
17. SECURITY CLASSIFICATION OF REPORT Unclassified	**18. SECURITY CLASSIFICATION OF THIS PAGE** Unclassified	**19. SECURITY CLASSIFICATION OF ABSTRACT** Unclassified	**20. LIMITATION OF ABSTRACT** UU

NSN 7540-01-280-5500 Standard Form 298 (Rev. 2-89)
Prescribed by ANSI Std. 239-18

THIS PAGE INTENTIONALLY LEFT BLANK

Approved for public release; distribution is unlimited

DETERMINATION OF THE PRESSURE EQUIVALENT NOISE SIGNAL OF VECTOR SENSORS IN A HYBRID ARRAY

Chuen Wah Kok
ME5, Republic of Singapore Navy
B. Eng., University of Adelaide, 2005

Submitted in partial fulfillment of the
requirements for the degree of

MASTER OF SCIENCE IN COMBAT SYSTEMS TECHNOLOGY

from the

NAVAL POSTGRADUATE SCHOOL
December 2012

Author: Chuen Wah Kok

Approved by: Daphne Kapolka
Thesis Advisor

Kevin B. Smith
Second Reader

Andres Larraza
Chair, Department of Physics

THIS PAGE INTENTIONALLY LEFT BLANK

ABSTRACT

The advent of particle velocity sensors as a viable addition to traditional pressure-based sensors in acoustics has fueled considerable research into the additional capabilities they might bring. Previous thesis work performed at NPS successfully demonstrated a working acoustic beamformer using a hybrid array comprised of a single conventional omnidirectional microphone and two 3D Microflown Ultimate Sound Probes in an anechoic chamber. These Microflown sensors are vector sensors. They have integrated directionality through the inclusion of three orthogonal particle velocity sensors with a microphone. Unfortunately, the signals of the particle velocity sensors obtained outside in a light, gusting wind were unusable due to broadband noise. Since the fundamental limit to detecting quiet targets depends on the noise floor, the aim of this thesis was to perform an in situ measurement of the pressure equivalent noise floor of all sensors in the array and to minimize the wind noise. Noise levels measured in an anechoic chamber were 9–15 dB higher than the levels expected from the sensors alone. The additional noise is attributed to the data acquisition equipment. The use of an ACO WS7 windscreen was shown to be extremely effective in mitigating broadband wind noise.

THIS PAGE INTENTIONALLY LEFT BLANK

TABLE OF CONTENTS

THIS PAGE INTENTIONALLY LEFT BLANK

LIST OF FIGURES

LIST OF TABLES

THIS PAGE INTENTIONALLY LEFT BLANK

LIST OF ACRONYMS AND ABBREVIATIONS

DAQ	Data Acquisition
EMI	Electromagnetic Interference
HDPE	High Density Polyethylene
LOFAR	Low Frequency Analysis and Recording
MRA	Maximum Response Axis
NPS	Naval Postgraduate School
PVL	Particle Velocity Level
SNR	Signal to Noise Ratio
SPL	Sound Pressure Level
USP	Ultimate Sound Probe
VSL	Velocity Spectrum Level

THIS PAGE INTENTIONALLY LEFT BLANK

I. INTRODUCTION

The advent of particle velocity sensors as a viable addition to traditional pressure sensors for acoustic signals raises the possibility of increased sonar array performance with smaller arrays. Caulk successfully demonstrated a working acoustic beamformer using a hybrid array comprised of a single conventional omnidirectional pressure microphone and two 3D Microflown Ultimate Sound Probe (USP) vector sensors in the anechoic chamber at the Naval Postgraduate School (NPS) [1]. These Microflown vector sensors contain a pressure sensor, i.e., microphone, in addition to three orthogonal particle velocity sensors. He performed an in situ calibration of the amplitude and phase of the array channels relative to the central microphone and then implemented the beamformer in the frequency domain. Under anechoic conditions his method was very successful. Unfortunately, the particle velocity sensors were unable to pick up any discernible target signal under field conditions with live, moving targets in high wind. The impulsive nature of the wind gusts resulted in wideband noise across much of the workable bandwidth [1].

The goal of this thesis was to establish the pressure equivalent noise floor of the particle velocity sensors under anechoic conditions and to examine the ability of windscreens to eliminate the wind noise previously noted. Knowledge of the noise floor of the individual sensors is the first step necessary to predict the fundamental limit of the array performance under conditions where ambient noise is negligible. The determination of this pressure equivalent noise floor required three main steps:

1. Obtaining the transfer function of each Microflown particle velocity sensor relative to its co-located pressure sensor across the frequency of interest.
2. Measuring the transfer functions of the Microflown pressure sensors relative to the calibrated conventional microphone.
3. Measuring the noise spectral density of the raw voltage signals of the Microflown channels in the anechoic chamber.

The examination of windscreen performance was conducted by measuring the output signals from one Microflown probe covered only with its original mesh cap simultaneously with the output of another one covered with an additional windscreen purchased from ACO Pacific Inc.

Microflown reports that the noise of the particle velocity sensors is dominated by thermal noise and also provides a nominal pressure equivalent noise spectrum level (NSL) with their calibration reports [2]–[6]. However, these figures do not take into account such factors as additional cabling, data acquisition equipment and any noise from the application of the measured transfer functions to determine the pressure equivalent signals of the particle velocity sensors.

The pressure equivalent noise spectrum levels measured in this thesis were 9–15 dB above the levels expected for both the conventional ACO microphone as well as the pressure and particle velocity channels of the Microflown vector sensors. The data acquisition (DAQ) equipment was determined to be the primary source of the additional noise. The ACO Pacific windscreens proved extremely successful at mitigating the broadband wind noise experienced in previous field work and are recommended as an essential addition to any signals recorded outside. Further work will need to be done to determine whether the electronic noise of the equipment is a limiting factor as compared to the quietest ambient noise levels expected. If so, it will be necessary to find DAQ equipment with a lower noise floor.

II. BACKGROUND

Much background information about the Microflown sensors including the historical development, theory, and applications can be found in the online Microflown E-book by Hans-Elias de Bree [7].

The Microflown acoustic particle velocity sensor developed out of research begun at the University of Twente in Holland in the mid-1990's when work began on using fluid flow devices to measure acoustic signals. The Microflown sensor is similar to a hot wire anemometer but uses the changing resistance of two closely-spaced heated wires instead of one to achieve directional sensitivity. When air flows in a direction across the two wires, heat convected from the first decreases the cooling in the second. Therefore, the resistance of the two wires changes by different amounts. If the difference in the resistance is measured, the signal is proportional to the component of air flow across the wires. On the other hand, air flow parallel to the wires results in the same change in resistance in both of them, and thus no difference signal is detected. The size and spacing of the wires is critical. They must have a low heat capacity for a quick response time. The wires must be close enough together for the heat to be convected from the upstream wire to the downstream, but not so close that significant amounts of heat can diffuse from the downstream wire back to its upstream counterpart [2]. The temperatures measured on the two wires in response to a particle velocity signal are shown in the graph below along with the difference and sum signals. The signal can be increased by 15–20 dB by packaging the particle velocity sensor in such a way that the air flow is funneled through a smaller orifice to increase it. This improvement, called packaging gain, improves the signal to noise ratio of the sensor because the noise is primarily electronic.

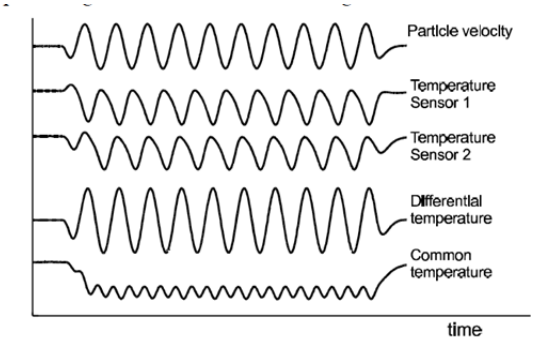

Figure 1. Temperature signal from Microflown sensor in response to acoustic signal (From [2])

Many different designs of the basic Microflown sensor have been produced, but the model used in this study was an Ultimate Sound Probe. This version has three nominally orthogonal particle velocity Microflown sensors as well as one co-located microphone. The particle velocity sensors consist of two 200 nm thick platinum wires over 150 nm silicon-nitride and spaced 5 μm apart. The wires are heated to between 200–400^{0}C [7].

A number of references in the Microflown library of publications discuss the self-noise features of these sensors. When implemented in the circuit shown in the figure below, the noise from the sensor itself is dominated by the thermal noise of the heated wires [3].

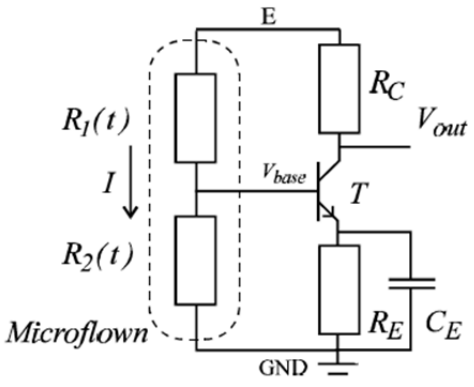

Figure 2. Typical circuit used to extract Microflown signal. $R_1 = R_2$ are the resistances of the heated wires (From [3])

The voltage signal produced by this thermal noise can be expressed as

$$e = \sqrt{2kT_s R\,Bw}\ , \tag{2.1}$$

where k is Boltzmann's constant, T_s is the temperature of the heated wire, R is the resistance of the wire, and Bw is the bandwidth over which the noise is measured. Since the signal is proportional to the change in resistance, the signal to noise ratio (SNR) is given by

$$\frac{S}{N} = \frac{I \cdot R\dfrac{\Delta R}{R}}{\sqrt{2kT_s R \cdot Bw}}\ , \tag{2.2}$$

where I is the current through the wires. Using the fact that the power dissipated in the wires is given by $P = I^2 R$, the formula above can be expressed as

$$\frac{S}{N} = \frac{1}{\sqrt{2k\,Bw}}\sqrt{\frac{P}{T_s}}\frac{\Delta R}{R}. \tag{2.3}$$

The conclusion of this analysis is that the SNR can be improved by increasing the length of the sensors to increase the power dissipated. The calculated self-noise for a one millimeter Microflown is $50\,dBre20\mu Pa$ in a 20 kHz A-weighted bandwidth. In contrast, the noise contribution of the preamplifier in the circuit was estimated as $0.5\,dBre20\mu Pa$. So the Johnson noise of the sensor wires themselves is expected to dominate overwhelmingly [3].

According to the Microflown E-book the lowest noise level of a typical Microflown particle velocity signal is about $-10\,dBre50\,{}^{nm}\!/_{s}$ in a 1 Hz bandwidth at 1 kHz [7]. The choice of reference velocity ($50\,{}^{nm}\!/_{s}$) makes the Sound Pressure Level (SPL) referenced to the standard $20\mu Pa$ roughly the same as the Particle Velocity Level (PVL) in air. This can be seen by calculating the particle velocity which corresponds to a pressure of $20\mu Pa$ to get

$$u = \frac{p}{\rho c} = \frac{20\,\mu Pa}{400 Pa \cdot s/m} = 50\,nm/s \text{ [4].} \qquad (2.4)$$

The values of air density, ρ, and sound speed, c, which make the particle velocity exactly equal to $50\,nm/s$ is about 4% lower than the accepted value at 20^0C of $415 Pa \cdot s/m$ [10]. This value of $-10\,dB re\,50\,nm/s$ is consistent with a graph of the measured electronic self-noise in a third octave bandwidth around 1 kHz of approximately $16\,dB re\,50\,nm/s$ [7]. Given that the bandwidth of a third octave at 1 kHz is 230 Hz, the integrated noise assuming a flat noise spectrum would be

$$VSL + 10\log\Delta f = PVL = -10\,dB re\,50\frac{nm}{s\cdot\sqrt{Hz}} + 10\log\frac{230Hz}{Hz} \cong 14\,dB re\frac{50nm}{s}\ , \qquad (2.5)$$

where VSL is the particle velocity spectrum level and Δf is the bandwidth.

A graph of the nominal noise floor of various Microflown sensors is given in the Calibration Reports included in Appendix B and is shown below. One can see that the self-noise of the velocity sensor of the USP is about 10 dB higher at 1 kHz than the self-noise of the "PU" sensor. This is due to the fact that the self-noise is expressed in terms of the equivalent PVL. The PU probes have a packaging gain due to the channeled flow of approximately 15 dB [2]. The noise voltage is divided by sensitivity to yield particle velocity. Therefore, the higher sensitivity of the PU probes yields a lower noise equivalent particle velocity assuming the same voltage noise. Although not explicitly stated, the scale of the graph is assumed to be the standard $dB re\,50\,nm/s\cdot\sqrt{Hz}$.

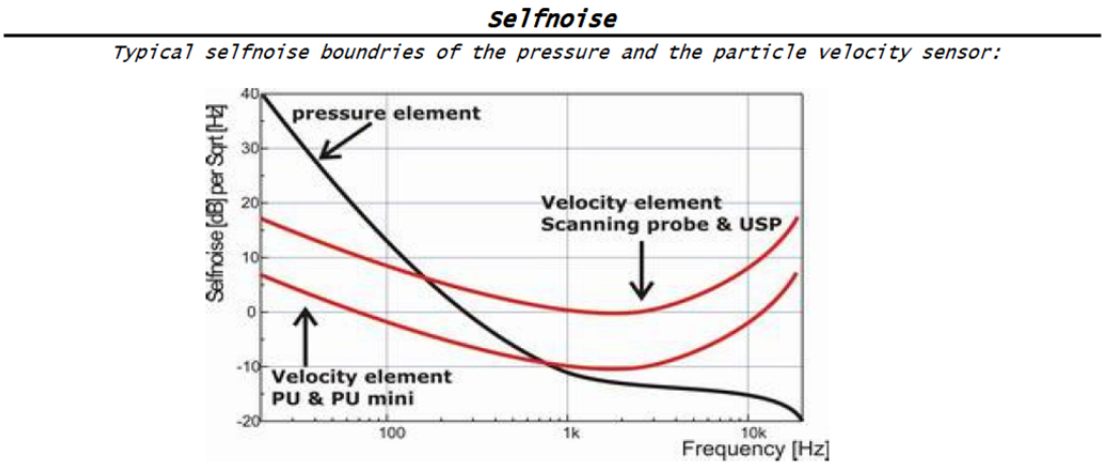

Figure 3. Nominal self-noise of Microflown sensors in dB re $20\mu Pa/\sqrt{Hz}$ or equivalently dB re $50nm/s/\sqrt{Hz}$ (From [5])

The voltage corresponding to a Velocity Spectrum Level of 0 dB can be found from the sensitivity of the particle velocity sensor. As an example, one of the particle velocity sensors had a calibrated sensitivity of 29.6 $V/m/s$ in high gain and 0.25 $V/m/s$ in low gain at 1000 Hz. This value was calculated using the nominal sensitivity at 250 Hz and the equation provided in [5]. We can adapt the standard definition of Pressure Spectrum Level to define the particle Velocity Spectrum Level (VSL) as

$$VSL \equiv 20\log\frac{\frac{u}{\sqrt{Hz}}}{\frac{u_{ref}}{\sqrt{Hz}}} = 20\log\frac{\frac{u}{\sqrt{Hz}}}{\frac{50\,nm/s}{\sqrt{Hz}}}, \tag{2.6}$$

A VSL of 0 dB corresponds to a particle velocity in a 1 Hz bandwidth of

$$u = 50\,nm/s \cdot 10^{0/20} \cong 50\,nm/s. \tag{2.7}$$

The voltage, e, in a 1 Hz bandwidth corresponding to this particle velocity when measured in high gain (the usual setting) can be found by multiplying by the sensitivity to get

$$e = 50\,{}^{nm}\!/_{s} \cdot 30\ {}^{V}\!/_{m/s} = 1.5\mu V \ . \tag{2.8}$$

Expressing this voltage in $dBre\,{}^{1V}\!/_{\sqrt{Hz}}$ yields

$$20\log\frac{1.5\mu V\,/\sqrt{Hz}}{1V\,/\sqrt{Hz}} = -116\,dBre\,{}^{1V}\!/_{\sqrt{Hz}} \ . \tag{2.9}$$

This is the approximate expected voltage noise spectrum level in a 1 Hz bandwidth at 1 kHz for a particle velocity channel of a USP.

A previous thesis student, CDR Jeff Caulk, built a hybrid array consisting of two Microflown USP sensors flanking a conventional ACO microphone [1]. The sensors were mounted in a holder with set screws to maintain orientation and set a distance of 17.2 cm apart to accommodate a 1 kHz design frequency for the array. The array design is shown below.

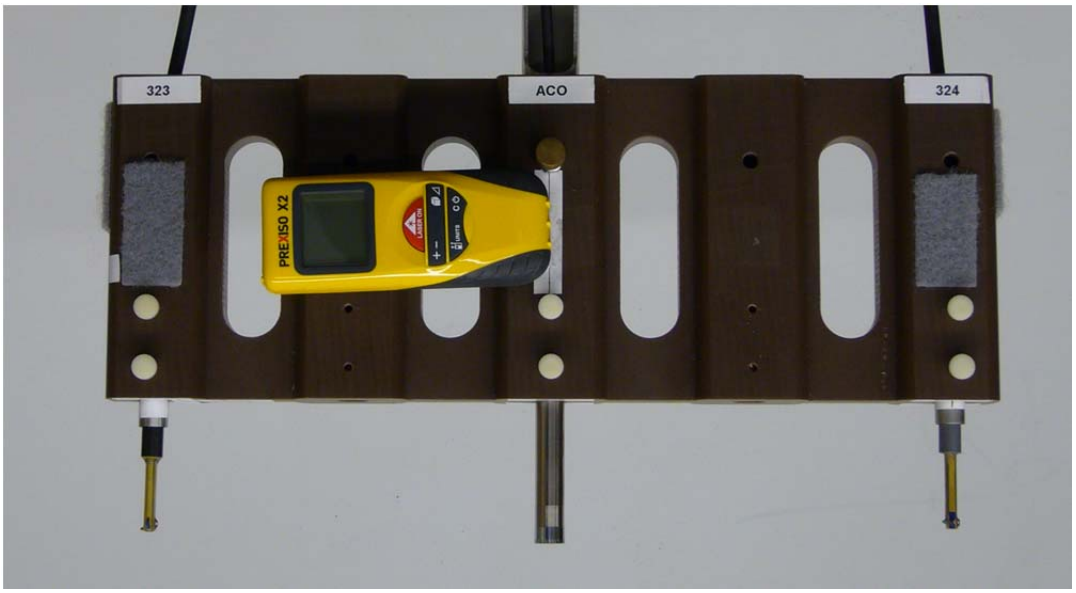

Figure 4. Hybrid array design showing central ACO microphone flanked by two Microflown USP sensors (From [1])

Instead of using the given calibration data for the sensors to determine signal amplitude and phase, Caulk measured the transfer functions in situ. There were two steps

to this process. First, he measured the transfer functions between each of the Microflown particle velocity channels along its Maximum Response Axis (MRA) and its co-located Microflown microphone. Then he measured the transfer functions between the Microflown microphones and the ACO microphone. In this way he was able to determine all transfer functions needed to successfully beamform the hybrid array.

The advantage of an array which includes vector sensors lies in its enhanced capability to determine directionality. This capability is due to the inherent directionality of the particle velocity sensors. The plot below shows the typical figure eight beampattern of Microflown particle velocity sensors.

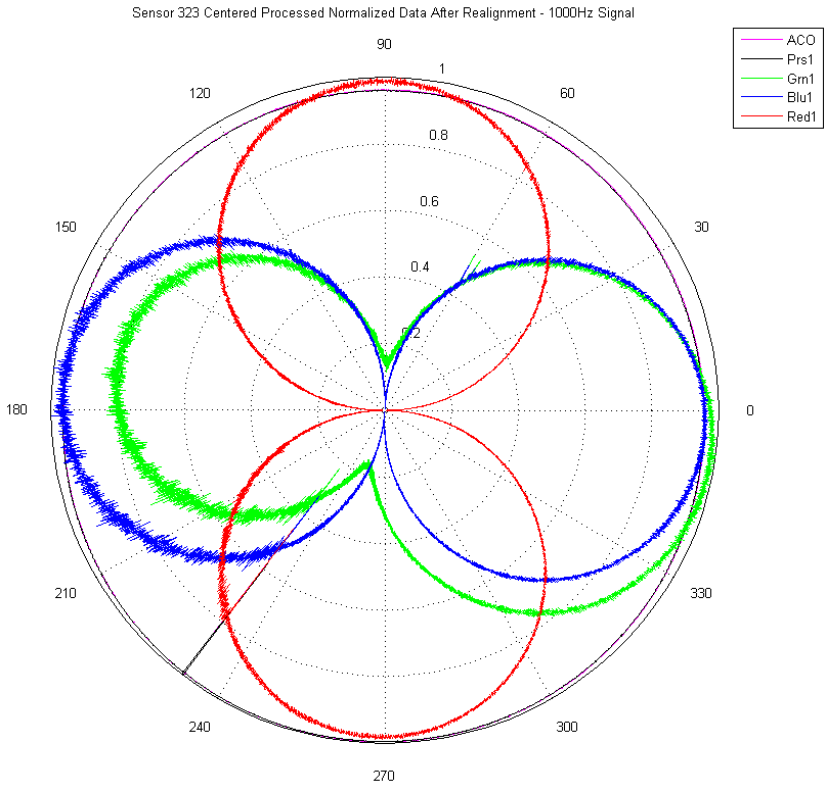

Figure 5. Beampattern of Microflown particle velocity sensors (From [1])

Using the results of the in situ calibration, a simple, linear beamformer was implemented in the frequency domain using the output of the particle velocity and pressure sensors of the array. The basic algorithm used followed the method described by Cray and Nuttall in their 2001 paper [8]. To test the beamformer performance, a

1 kHz sound source was activated in the far field of the array and the signal recorded in each of the hybrid array channels. The beamformer output based on the three pressure sensors of the hybrid array is shown on the left in the diagram below. The finite aperture of the linear array of omnidirectional pressure sensors allows for a determination of the polar angle of a source, but the azimuthal angle is completely undetermined due to the symmetry of the linear array. In contrast the beamformer output using both pressure sensors and particle velocity sensors is shown on the right. The directionality of the particle velocity sensors allows a determination of the azimuthal as well as polar angle of the source relative to the array.

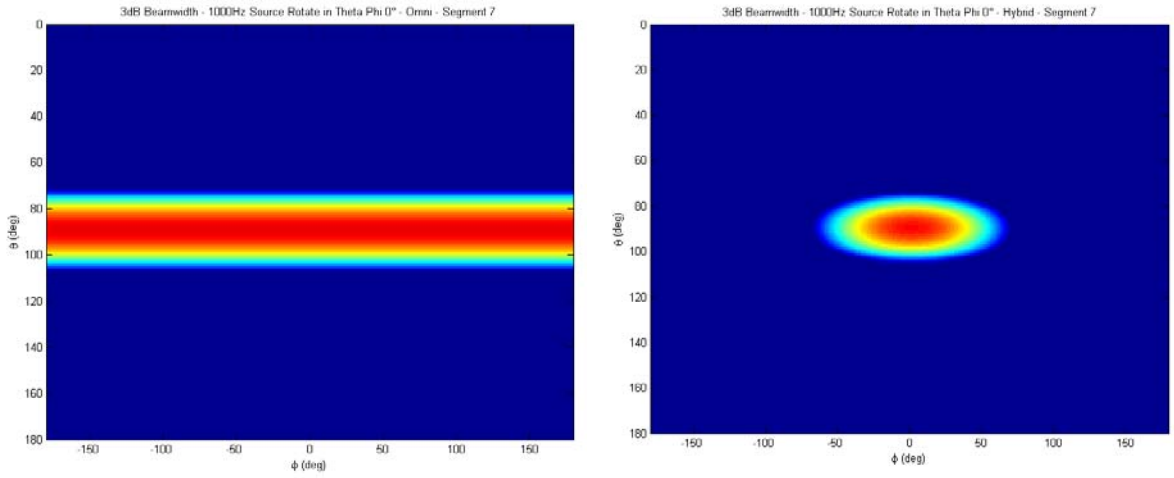

Figure 6. Beamformer output of array with 1 kHz source using pressure sensors alone (left) and using both pressure and particle velocity sensors (right) (From [1])

After examining the performance of the hybrid array in the anechoic chamber with a variety of sources and frequencies, Caulk next attempted to use the array under more realistic conditions. He collected signals from passing aircraft on the roof. The sensitivity of the particle velocity sensors to gusting wind can be seen in the Low Frequency Analysis and Recording (LOFAR) grams below. LOFARgrams are plots of the frequency spectra of signals as a function of time. Time is usually on the vertical axis and presented in a waterfall display with the newest data on the top.

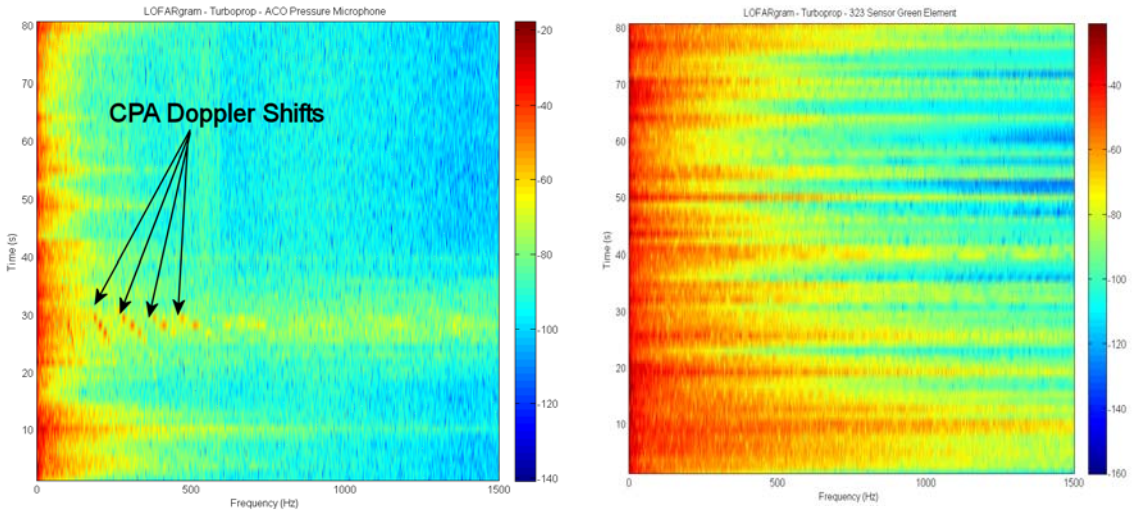

Figure 7. LOFARgram of overflying plane of microphone output (left) and particle velocity output (right) (From [1])

As can be seen from the LOFARgram, the impulsive nature of the gusting wind resulted in substantial noise components across a wide frequency band. The plots show frequency from DC to 1500 Hz. The majority of the signal from the aircraft is below 500 Hz. Therefore, it was impossible to successfully beamform the hybrid array with the particle velocity sensors due to their sensitivity to wind noise. This experience led to the desire to get better windscreens for the array sensors as well as to carefully characterize the noise floor of the Microflown sensors as measured with the actual array and processing scheme.

THIS PAGE INTENTIONALLY LEFT BLANK

III. THEORY

This chapter covers the definition of directions related to the hybrid array, the details of the transfer function measurements, and the algorithm used to determine the pressure equivalent noise level of the Microflown particle velocity sensors.

A. HYBRID ARRAY COORDINATE SYSTEM

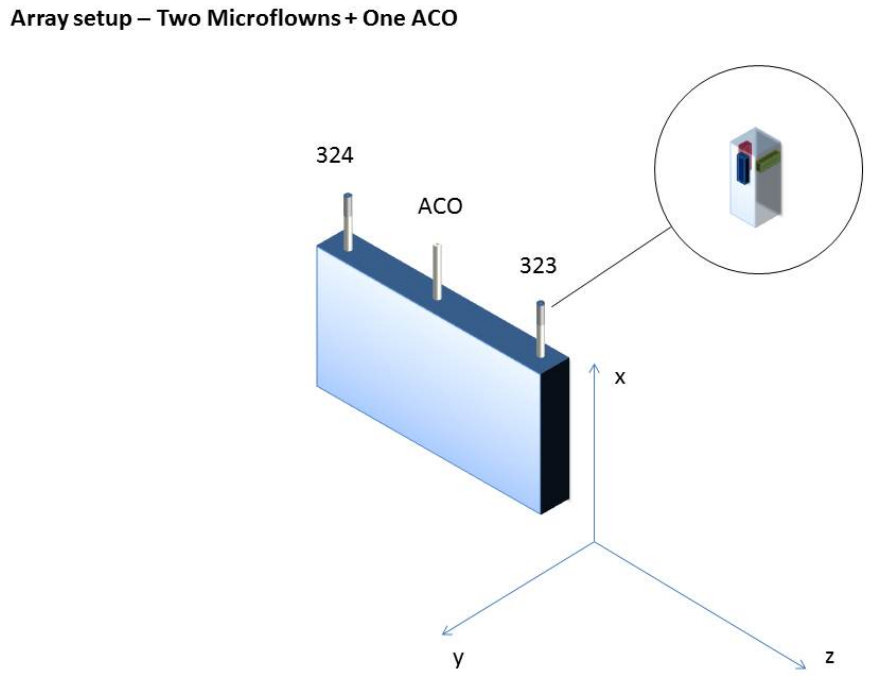

Figure 8. Hybrid Array Setup

Figure 8 illustrates the directions defined in terms of the hybrid array. As in Caulk's work, it consists of an ACO Pacific microphone in the middle of the array flanked by two Microflown Ultimate Sound Probes on each side designated as sensor 323 and 324. The array was designed with the frequency of interest centered at 1 kHz, with a corresponding wavelength of about 34 cm. To form an array with elements spaced at half-wavelength intervals, each of the sensors are set 17.2 cm apart in the array fixture

which is aligned with the *z*-axis. Straight up above the sensors is the *x*-direction, and the *y*-direction is perpendicular to the largest side of the holder to form a right-handed coordinate system.

The Microflown probes have a wire mesh screen encasing a set of four sensors. An omnidirectional pressure sensor is centered on the top of the probe, and three particle velocity sensors are oriented to detect acoustic particle flow in three orthogonal directions. The manufacturer designates these particle velocity sensors as the GREEN, RED and BLUE elements. In this application, the particle velocity sensors were positioned along the *x*, *y* and *z* axes of a right-handed Cartesian coordinate system as shown in Figure 9. The MRA of the green sensor is along the *x*-axis. The MRA of the blue sensor is in the *z*-direction, and the MRA of the red is in the *y*-direction. The polar angle, θ, is defined as the angle from the *z*-axis, and the azimuthal angle, ϕ, is the angle measured counter-clockwise from the positive *x*-axis.

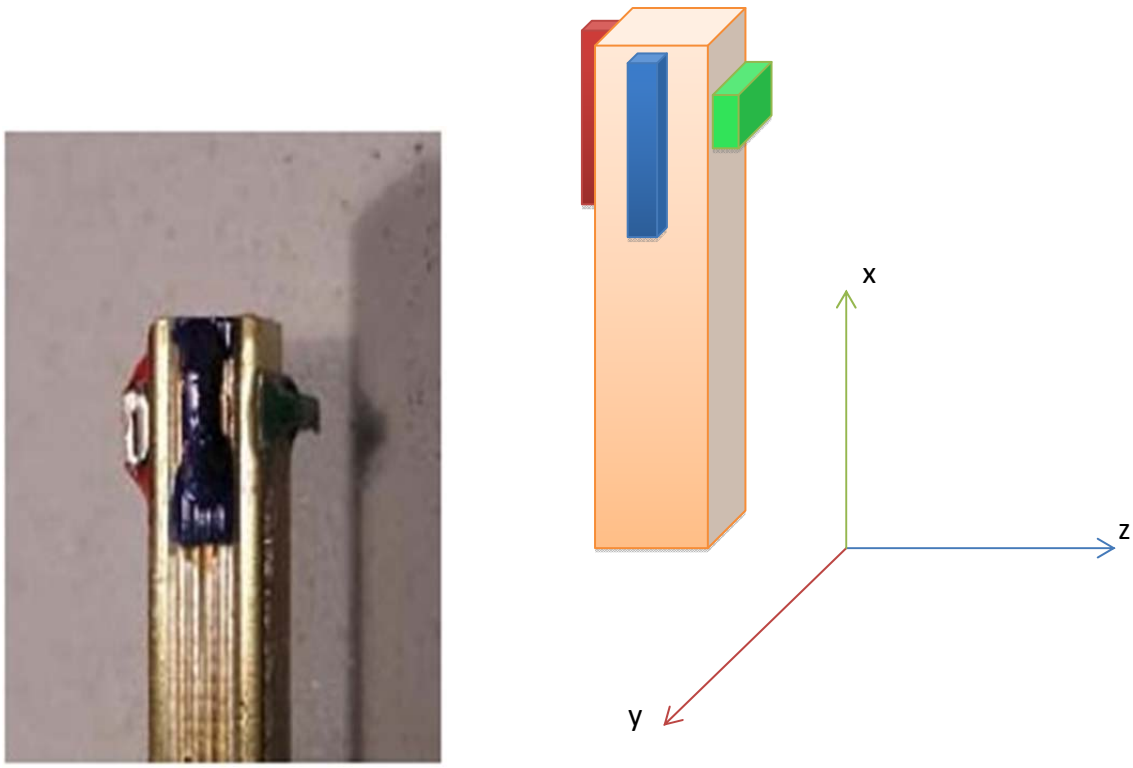

Figure 9. Microflown Ultimate Sound Probe without endcap showing sensor orientation

Figure 10. Microflown Ultimate Sound Probe with endcap

B. DETAILS OF TRANSFER FUNCTION COMPUTATION

In order to beamform an array, the relative amplitude and phase responses of the individual sensors need to be known. Although the ACO Pacific and Microflown Technologies manufacturers both provide calibration data of the equipment, application of calibration data does not take into account the acoustic interaction due to the physical proximity of the sensors and fixture of the array. It also does not take into consideration any amplitude and phase variations due to the cabling and the DAQ equipment used. Therefore, following the procedures developed in [1], an in situ calibration of the entire array was accomplished in the frequency domain by obtaining the transfer functions between each channel of the Microflown sensors with a common reference sensor in the array, i.e., the centrally positioned ACO Pacific microphone.

The transfer functions are measured in the far-field of the array where the acoustic particle velocity is related to pressure by

$$u = \pm \frac{p}{\rho c}. \tag{3.1}$$

As such, the amplitude of the acoustic particle velocity differs by a factor of ρc from the pressure. It is either in phase with the pressure or 180^0 out of phase depending on whether the wave is traveling in a positive direction relative to the velocity sensor or in the negative direction. To determine the transfer functions between the pressure and particle velocity channels, the MRA of the velocity sensor needs to be pointed towards

the acoustic source. The amplitude response of the particle velocity sensor falls off as the cosine of the angle between the sensor's MRA and the particle velocity direction. The diagram below shows the MRA of the BLUE particle velocity sensor along with a snapshot of the particle velocity during a compression. For sound coming from the directions of $+\hat{z}$, the BLUE particle velocity response will be maximum and out-of-phase with pressure. In other words, during a compression, the particle velocity will be in the negative direction. For sound coming from $-\hat{z}$, the response will be a maximum and in-phase with pressure. For sound coming from the $-\vec{u}$ direction, the response is proportional to the cosine between $\vec{u}$ and $\hat{z}$, i.e., $\cos\theta$. This is the direction cosine between the direction of sound propagation and the *z*-axis. The phase of the particle velocity relative to the pressure is taken care of by this term as well.

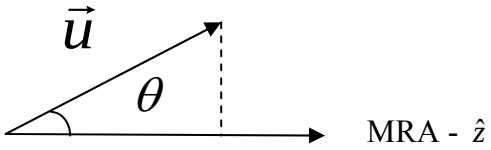

Figure 11. Particle velocity response proportional to the direction cosine between actual particle velocity direction and MRA

In a similar way, the response of the particle velocity sensors with MRAs in the *x*- and *y*-directions are proportional to the direction cosines of the negative of the sound propagation direction and their MRAs. With the polar and azimuthal angles defined above, these direction cosines are

$$\theta_x = \frac{\vec{u}}{u}\cdot\hat{x} = \sin\theta\cos\phi,\ \theta_y = \frac{\vec{u}}{u}\cdot\hat{y} = \sin\theta\sin\phi, \text{ and } \theta_z = \frac{\vec{u}}{u}\cdot\hat{z} = \cos\theta\ . \tag{3.2}$$

As mentioned earlier, the measurements of the transfer functions need to be accomplished in two stages

1. Attaining the transfer function between each of the velocity sensors relative to the pressure sensor on the same Microflown probe along the MRA of the velocity sensor.

2. Attaining the transfer function between of the pressure sensor of the Microflown probes and the ACO microphone.

For stage one, three sets of transfer functions are required for each Microflown probe since they house three particle velocity sensors. Because the pressure sensor is co-located in the probe, amplitude and phase differences of the acoustic wave are minimized between the sensors. As an example, the transfer function between the pressure sensor and the BLUE particle velocity sensor is given by

$$\hat{H}_{1b}(k) = \frac{\hat{X}_{1p}(k)}{\hat{X}_{1b}(k)}, \tag{3.3}$$

where

- $\hat{H}_{1b}(k)$ is the transfer function between pressure and BLUE velocity sensor as a function of the bin frequency (k).
- $\hat{X}_{1p}(k)$ is the complex discrete Fourier transform of microphone signal of the 323 Microflown probe.
- $\hat{X}_{1b}(k)$ is the complex discrete Fourier transform of the BLUE particle velocity signal of 323 Microflown probe.

Upon establishing these transfer functions, the output of each velocity sensor can be properly scaled to the probe pressure sensor as follows. Take the complex discrete Fourier transform of the velocity sensor and multiply by the measured transfer function between pressure and particle velocity to get the corrected particle velocity

$$\hat{X}_{1bc}(k) = \hat{H}_{1b}(k)\hat{X}_{1b}(k). \tag{3.4}$$

The scaled velocity component is now matched to the pressure component in terms of both amplitude and phase. Its amplitude will be less than the pressure signal if the direction of sound was not along the MRA, and it will either be in-phase with the pressure signal or 180° out-of-phase depending on whether the direction cosine is positive or negative.

The next step is to establish the transfer function between the ACO microphone and the pressure signals of the two Microflown probes. When the three sensors are located an equal distance away from the acoustic source in the far field region, they see a

signal of equal pressure and phase. The transfer function of the ACO reference to the first Microflown pressure element is expressed as

$$\hat{F}_{21}(k) = \frac{\hat{X}_2(k)}{\hat{X}_{1p}(k)}, \tag{3.5}$$

where $\hat{X}_2(k)$ is the discrete Fourier transform of the ACO microphone. Using this, the BLUE particle velocity signal from the 323 probe can be corrected to an equivalent ACO value as

$$\hat{X}c_{1b}(k) = \hat{F}_{21}(k)\hat{H}_{1b}(k)\hat{X}_{1b}(k). \tag{3.6}$$

All of the Microflown particle velocity and pressure channels can be "corrected" to the equivalent ACO values in the same way. These "corrected" signals are the voltage signals which would appear on the ACO microphone output for an acoustic signal equal to the one seen by each of the Microflown channels. Because the amplitude and sign of the particle velocity signals varies with the direction cosine, their "corrected" values also contain this cosine dependence. In this way all corrected outputs have signals that are commensurate with the ACO microphone.

C. DETERMINATION OF PRESSURE EQUIVALENT SIGNAL

Since the transfer functions enable the scaling of the pressure and velocity signals to the voltage signal measured by the ACO microphone, knowledge of the ACO sensitivity allows the Microflown pressure and velocity signals to be expressed in terms of acoustic pressure. By capturing signals from each of the Microflown channels in the absence of acoustic sound, the noise floor of the sensors can be determined and expressed in terms of its pressure equivalent. When the channels of the array are later beamformed to detect a contact and determine its bearing, all raw output signals are similarly "corrected" by use of these transfer functions. Therefore, this technique captures the actual measured noise in the beamformer channels in units of pressure.

If the ACO microphone reference pressure sensitivity, M_2, is a constant across the frequency band of interest then the pressure equivalent of the ACO channel in the frequency domain can be expressed as

$$\hat{P}_2(k) = \frac{\hat{X}_2(k)}{M_2} \ . \tag{3.7}$$

Thus the transfer function of the Microflown pressure sensor to the ACO reference in pressure equivalent becomes

$$\hat{F}_{P1}(k) = \frac{\hat{X}_2(k)}{M_2 \hat{X}_{1p}(k)} = \frac{\hat{F}_{21}(k)}{M_2}. \tag{3.8}$$

The corrected pressure signal of the Microflown 323 pressure sensor can then be calculated as

$$\hat{P}_{1p}(k) = \hat{F}_{P1}(k)\hat{X}_{1p}(k). \tag{3.9}$$

Similarly, the corrected pressure equivalent of the individual Microflown particle velocity sensors can be obtained through the product of the transfer functions. Taking the 323 Microflown BLUE particle velocity sensor as an example, the corrected pressure equivalent value in the frequency domain is given by

$$\hat{P}_{1b}(k) = \hat{F}_{P1}(k)\hat{H}_{1b}(k)\hat{X}_{1b}(k). \tag{3.10}$$

THIS PAGE INTENTIONALLY LEFT BLANK

IV. TRANSFER FUNCTION MEASUREMENTS

A. EQUIPMENT SET UP

Measurements to determine the pressure equivalent noise floor were carried out in an anechoic chamber to minimize ambient acoustic noise and reflections. The National Instruments Compact Data Acquisition chassis and supporting modules is the principle interface for data extraction and digitalization from the ACO microphone and two Microflown Ultimate Sound Probes [9]. LABView and MATLAB software were used to process the data.

To obtain the transfer function, broadband white noise source from a function generator was fed to an Austin amplifier positioned well into the far field at 2 m from the array. Equipment settings for these measurements are listed in Table 1.

S/N	Equipment	Settings	Level	Remarks
1.	HP Function Generator	Source	Noise	
		Voltage	5 Vpp	
2.	Austin Amplifiers	Master Volume	Max	
		OD Volume	Max	OD ON
		Gain	0	
3.	Microflown Signal Conditioner	Gain	High	
		EQ	OFF	EQ switched on would result in a flat phase response

Table 1. Equipment Settings

The equipment used is listed below. The Calibration Report for the 324 Microflown USP is provided in Appendix B. Appendix C contains the calibration data

for the ACO microphone, and Appendix D has an excerpt from the specifications for the data acquisition module, NI 9234, which shows its expected noise floor confirming the conclusion that the noise floor is dominated by the DAQ equipment. Appendix E shows the expected attenuation resulting from using an ACO WS7 windscreen.

- ACOustical Interface Pacific Calibrated Pressure microphone – Cartridge Model 7046
- ACOustical Interface Pacific 1/2" preamplifer – Model 4012
- ACO WS7 Untreated windscreen
- Microflown Holland Ultimate Sound Probe – Model UT0901-23 (x2)
- Microflown Holland Ultimate Sound Probe 4 Channel Signal Conditioner – Model E0901-23 (x2)
- National Instruments Compact DAQ USB Chassis – Model NI 9172
- National Instruments Sound and Vibration DAQ Module – Model NI 9234 (3x)
- Function Generator
- Austin Speaker
- Johnson Self Leveling Laser Level – Model 40-6620
- Chamber rotator
- Software: LabVIEW version 2011
- Software: MATLAB R2008b

The hybrid array had an effective array aperture of 34.4 cm, and the source had a radius of about 10 cm. For an incident wave to be well-approximated as a plane wave across the array aperture, the distance from the source should be a minimum of the far field range [10].

$$FF = \frac{L^2}{4\lambda} = \frac{\left(0.344m\right)^2}{4 \cdot \frac{343\frac{m}{s}}{1000Hz}} \cong 9cm \tag{4.1}$$

As all data collection was done with the Austin speaker positioned 2 m from the array, the far field requirements were well satisfied. The distance was also far enough to

ensure that the pressure and particle velocity of the sound were in-phase at the lowest usable frequencies (about 200 Hz). This phase relationship requires that the wavenumber times the range be greater than one [10]. At a range of 2 m, the value of kr at 200 Hz is about 7. At higher frequencies, the value of kr would be even higher.

The transfer function needs to account for the effect of the proximity of the sensors as positioned in the array holder, as well as disturbances introduced by the array holder itself. As such the transfer function signal data was collected with all the sensors affixed to the array. The array holder is constructed from High Density Polyethylene (HDPE) plastic. The mass of the array attached by rigid clamps to the stand helps to damp out high frequency vibration induced noise signals. The relatively large aspect presented by the array in the *y*-direction and close proximity to the sensor elements' *x*-axis may introduce significant reflections. In effort to minimize these reflections, foam paddings were attached to exposed surfaces of the holder as shown in the figure below.

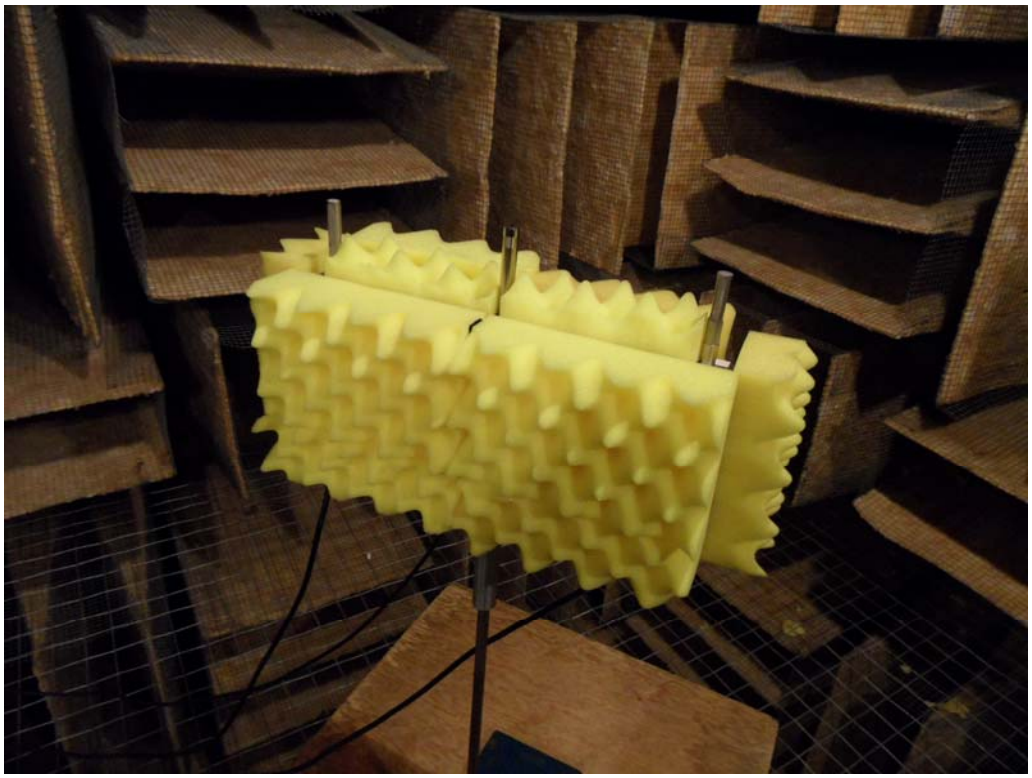

Figure 12. Foam padding to minimize reflection from holder

B. POSITIONING THE SENSORS AND ARRAY

The Microflown probes are constructed without physical slots or keyways for alignment of the particle velocity sensors. A marking of the relative axis on the RED element direction is the only reference for positioning of the particle velocity sensor axis. Therefore the probe's particle velocity to the array axis is aligned by sight and secured in place by hand tightening of a screw. Fortunately, the particle velocity response changes very gradually about its MRA, so this method had been proven previously to provide acceptable results [1]. Once in place, the holder keeps the sensors in a fixed relative alignment for the measurement of the transfer functions. If any of the sensors are removed or rotated, a new set of transfer function needs to be calculated.

To obtain accurate transfer functions, good phase coherence between the sensors of interest is critical. The signal along the velocity sensor's MRA is the strongest and therefore yields the best coherence for the particle velocity sensors. Therefore the noise source is placed in a static position directly along the MRA of the sensor of interest at a distance of 2 m for data acquisition. Because the two Microflown probes each contain three particle velocity sensors, a total of six transfer functions are needed between the Microflown pressure and particle velocity sensors. Since the two probes are lined up in the *z*-axis direction along the BLUE MRA, only five positions are needed to establish these transfer functions. Both Microflown probes are measured concurrently along the positive BLUE direction. Figure 13 illustrates the positioning of the noise source for measurement of the BLUE MRA measurement for both the 323 and 324 probe.

Figure 13. Positioning of noise source for BLUE MRA measurement (shown with windscreen attached)

Initially, data for the GREEN MRA was gathered with the array holstered in the ceiling mounted rotator of the anechoic chamber, with the speakers placed directly below the Microflown probe of interest. Distance in this configuration between the sensors and noise source is reduced to 1.33 m, which is still in the far field range. Figure 14 shows the positioning of the speaker with respect to the array. However, as explained later, this arrangement appeared to result in reflections. Therefore, the final transfer functions were obtained with an alternative arrangement.

Figure 14. Initial measurement of sensor 323 along the GREEN MRA

C. CALCULATION OF TRANSFER FUNCTION

The data collected was post processed using MATLAB software to obtain the transfer functions. Data was collected in blocks of 2 min with a sampling frequency of 4267 Hz. Data was processed in packets of 1024 data points and averaged with 50% overlap to increase the signal to noise ratio, followed by application of Hanning windows to reduce frequency smearing. A total of 250 averages were obtained in the two minute intervals. The measurements were repeated three times.

The coherence of the signal pairs used to calculate each transfer function was checked to verify that sufficient signal to noise level was present to obtain a valid transfer function. It was calculated using the *mscohere* function in MATLAB [11].

In the absence of noise, the transfer function between two discrete signals, $x(n)$ and $y(n)$ can be estimated as the ratio of their discrete Fourier transforms.

$$\hat{H}(k) = \frac{\hat{Y}(k)}{\hat{X}(k)}. \tag{4.2}$$

However, in the presence of noise, it is necessary to average to increase the signal to noise. In this case, the transfer function can be estimated as

$$\hat{H}(k) = \frac{\sum_{n=1}^{M} \hat{Y}(k)\hat{X}^{*}(k)}{\sum_{n=1}^{M} \hat{X}(k)\hat{X}^{*}(k)}, \qquad (4.3)$$

where M is the number of averages. This method was implemented in MATLAB by taking the ratio of the average cross power spectral density using the *cpsd* function to the power spectral density using the *psd* function. Both of these estimates are based on Welch's Method [11].

D. TRANSFER FUNCTION FROM MICROFLOWN PRESSURE TO PARTICLE VELOCITY

MATLAB was used compute the transfer functions between the Microflown sensor elements and the ACO microphone pressure sensor. The transfer functions between the Microflown pressure sensor and the particle velocity sensors were computed first and some representative results are shown in Figures 15 and 16 below. A total of three data sets were collected for each transfer function to check the consistency. The results of all three trials are shown in these graphs.

The transfer function between the 323 Microflown pressure sensor and the GREEN particle velocity sensor exhibited significantly greater fluctuations compared to the RED and BLUE channel. These fluctuations are thought to be the result of reflections from the ceiling mounted rotator structure. The array was mounted on it for the GREEN MRA measurement. When the array was repositioned horizontally with a clamp standing on the floor of the chamber, the fluctuations were absent from the revised transfer function as shown in Figure 17. The new revised positioning was used for the remainder of the GREEN transfer function measurements.

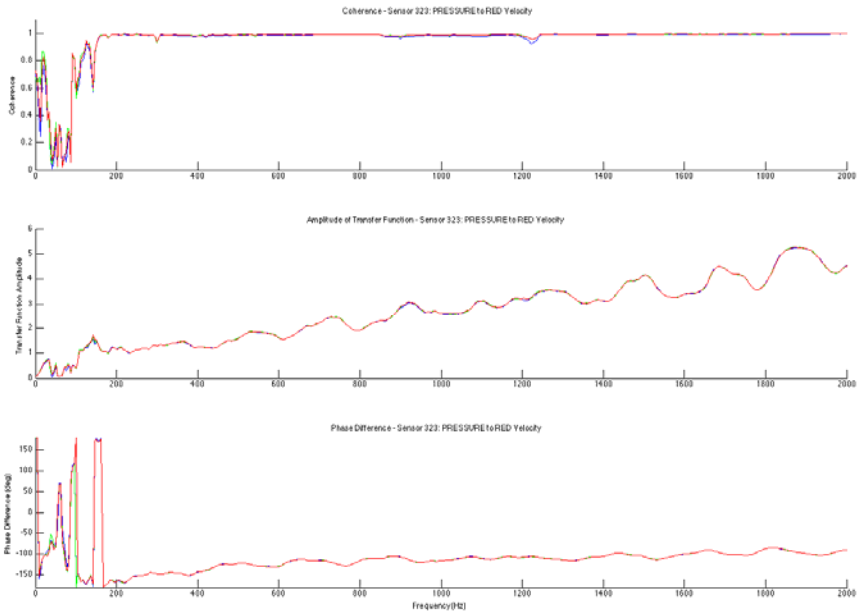

Figure 15. Transfer function of 323 RED particle velocity sensor to Microflown pressure sensor

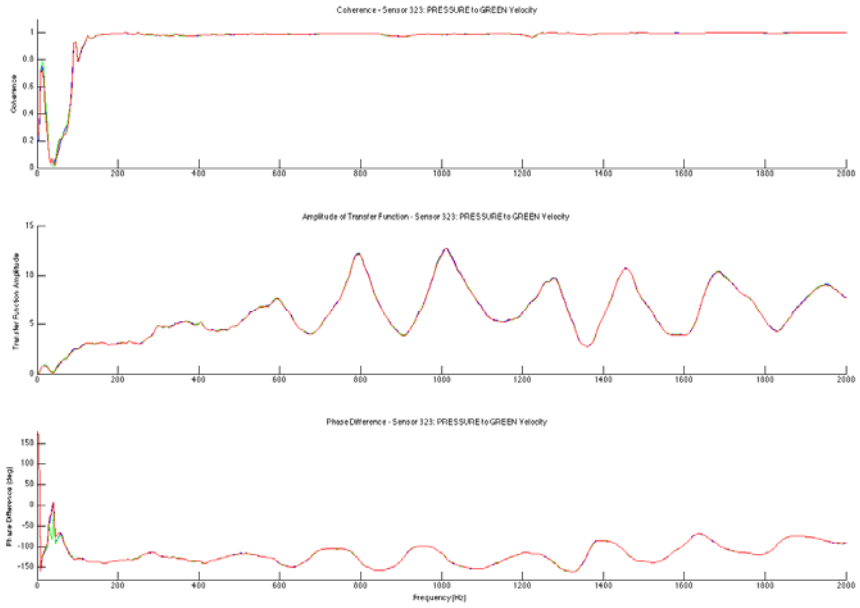

Figure 16. Transfer function of 323 GREEN particle velocity sensor to Microflown pressure sensor showing considerable periodic variations in amplitude and phase. This data was obtained with array holstered in ceiling mounted rotator

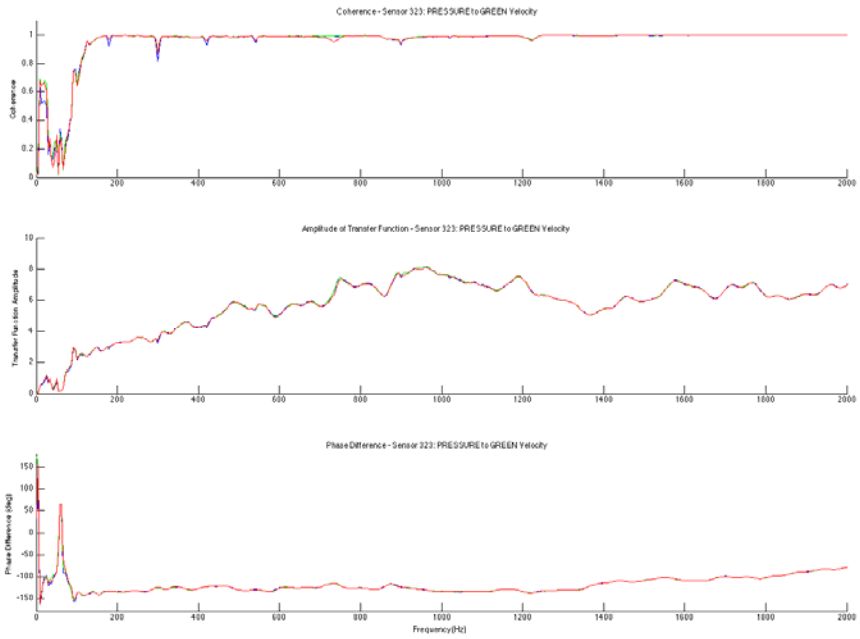

Figure 17. Revised transfer function of 323 GREEN particle velocity sensor to Microflown pressure sensor. This data was obtained with the array repositioned horizontally

The transfer functions obtained show a consistent response of the onboard pressure to particle velocity elements above 200 Hz where there is good coherence. The lack of coherence below 200 Hz may be the result of limited acoustic power projected by the Austin speakers at these low frequencies, noise from convection currents in the chamber, and/or electronic noise. Since the sensitivity of the Microflown particle velocity sensors rolls off at low frequencies, the signal to noise decreases in this regime as shown in Appendix B.

The shape of the transfer functions for the RED and BLUE elements were similar. They both showed a slow increase of amplitude with frequency. The GREEN element was not as consistent. Figure 17 shows a decline in the amplitude with frequency after about 1 kHz. It is possible that the top edge of the holder caused additional reflections that may have affected the transfer function curve despite the addition of foam to minimize these reflections.

The excellent agreement between the three separate measurements of these transfer functions was examined in more detail. As an example, the fractional uncertainty in the transfer function amplitude between the 324 microphone and the BLUE particle velocity element was less than 2% across the useable frequency range. This is shown in Figure 18. Similar results were obtained with the phase of the transfer function which is critical to beamforming success. As shown in Figure 19, the standard deviation of the three measurements revealed less than one degree uncertainty in phase.

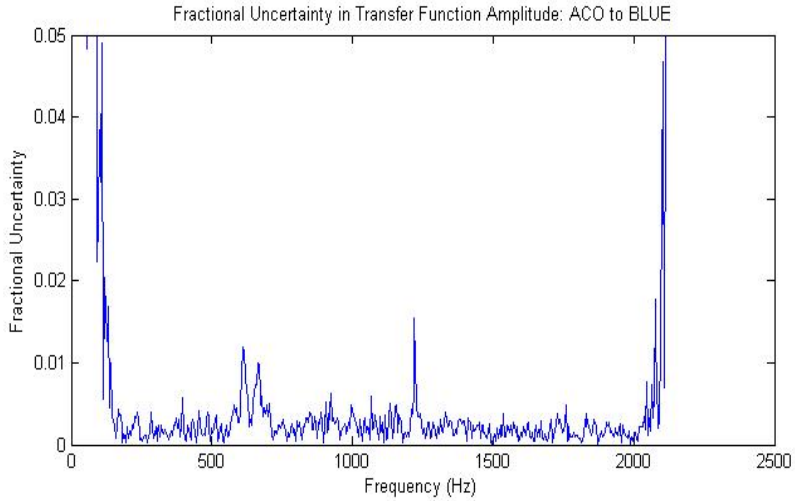

Figure 18. Fractional uncertainty in transfer function amplitude

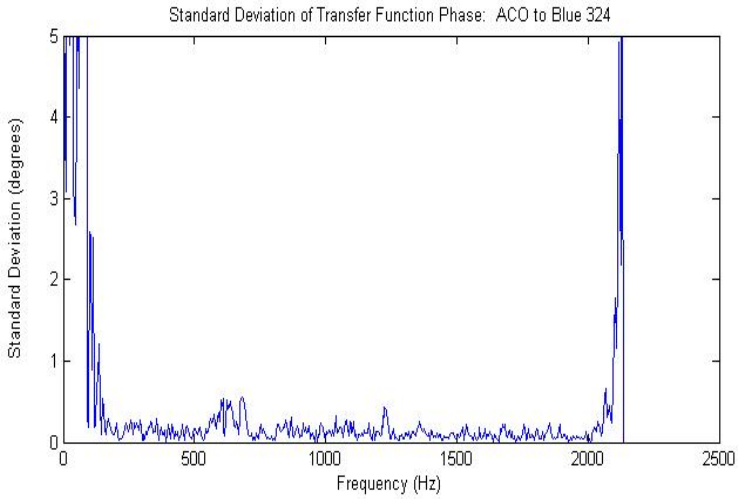

Figure 19. Fractional uncertainty in transfer function phase

E. TRANSFER FUNCTION FROM ACO MICROPHONE TO MICROFLOWN PARTICLE VELOCITY ELEMENTS

In order to reference individual particle velocity elements to the ACO microphone, the transfer function of the Microflown microphone to individual particle velocity element must be multiplied by the transfer function of the ACO microphone to Microflown microphone as explained in the Chapter III.

The transfer functions between the 323 Microflown pressure sensors and the ACO microphone are shown in the figures below. As before, three sets of data were obtained and then averaged. As an added precaution, the transfer functions were measured along the MRA of the particle velocity channel they were to be used for. Again there is excellent agreement between the trials. Apparent phase discontinuities in the some of the transfer functions are "folded over" due to representation of the phase where the vertical axis ranges from –180° to 180°. The differences in these transfer functions are fairly small but probably worth measuring them on the MRA of the particle velocity channel they are to be used for. These small differences may be due to diffraction, reflection, and/or the slight differences in source distance for the different orientations.

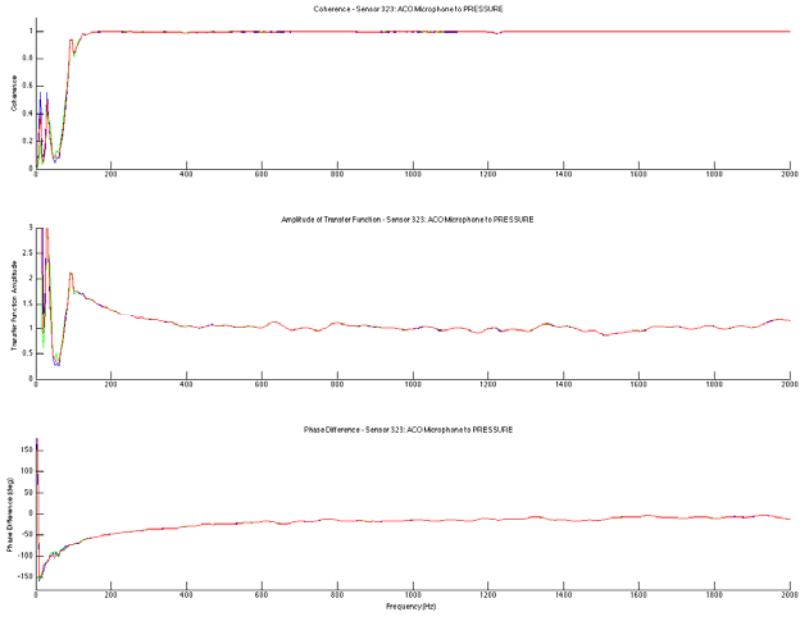

Figure 20. Transfer function from ACO microphone to 323 pressure sensor measured on RED MRA

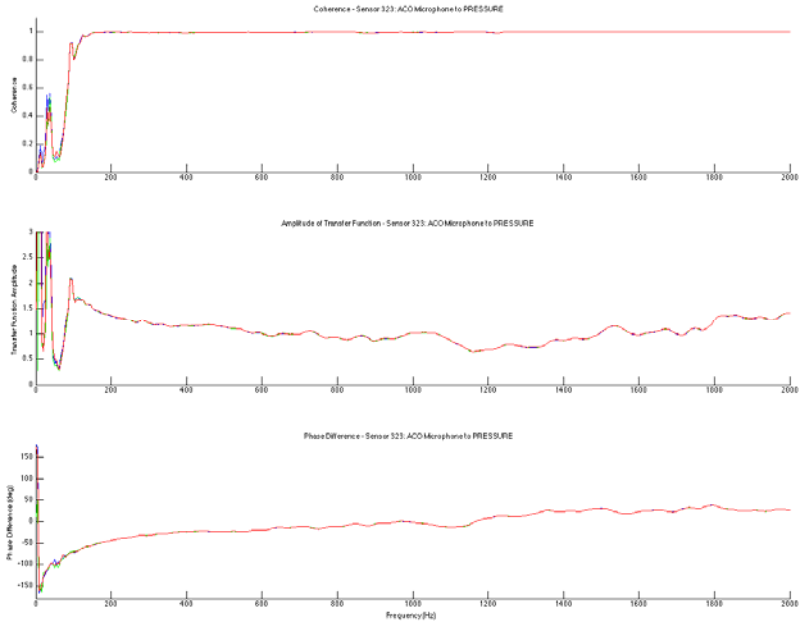

Figure 21. Transfer functions from ACO microphone to 323 pressure sensor on GREEN MRA

The final transfer functions between the ACO microphone and particle velocity elements were obtained by multiplying the two average transfer functions. The final composite transfer functions between the ACO microphone and the 324 particle velocity sensors are shown below.

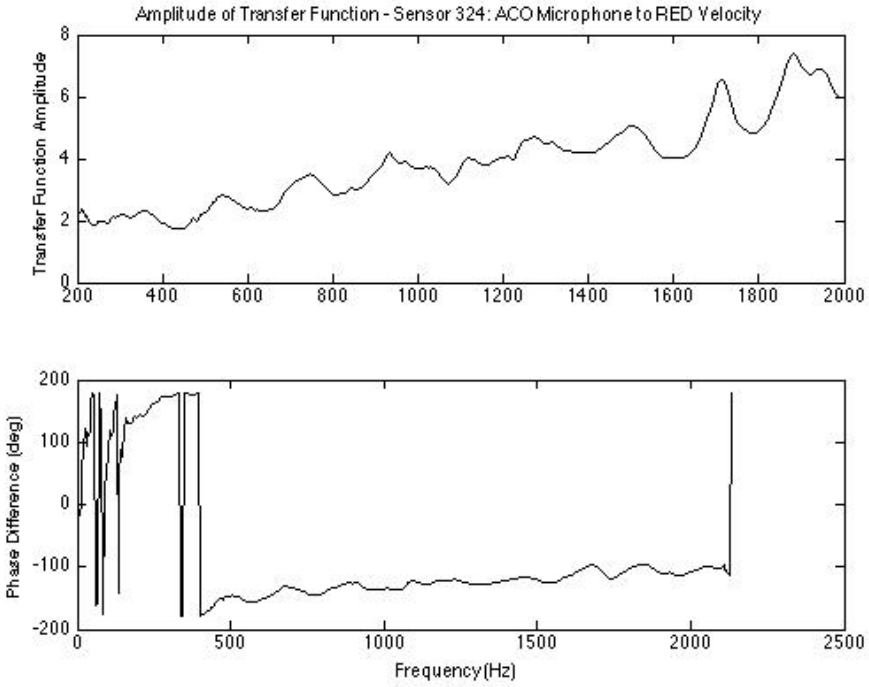

Figure 22. Final transfer function from ACO microphone to 324 RED particle velocity sensor

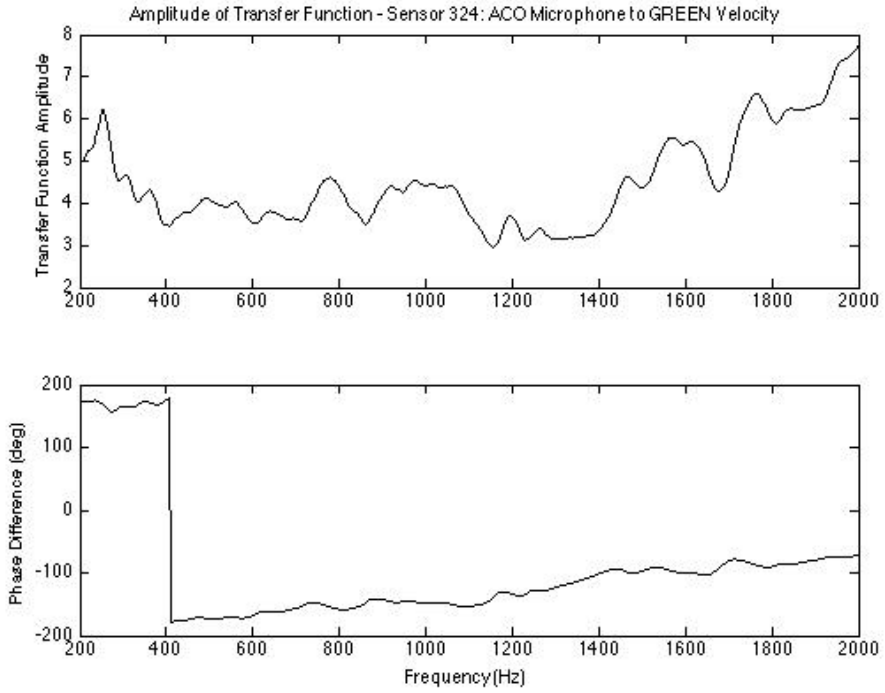

Figure 23. Final transfer function from ACO microphone to 324 GREEN particle velocity sensor

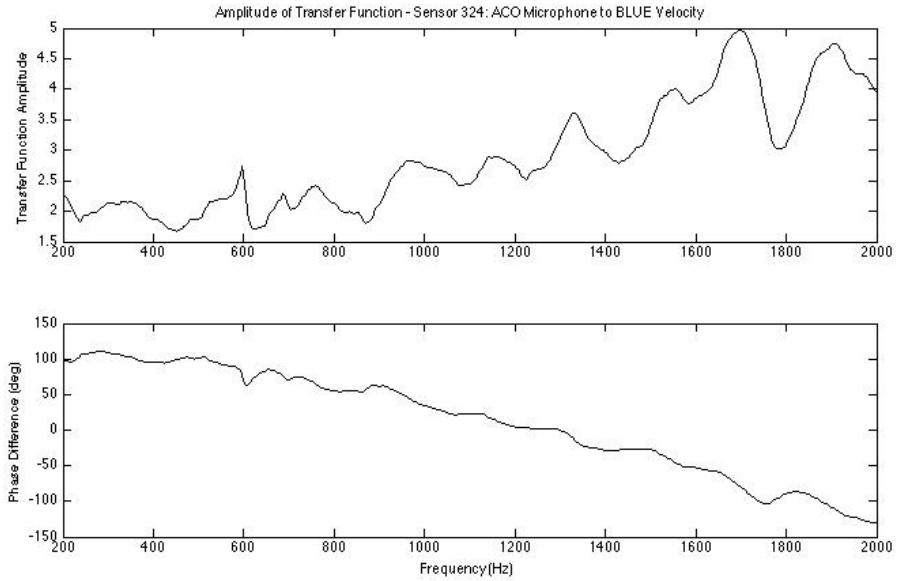

Figure 24. Final transfer function from ACO microphone to 324 BLUE particle velocity sensor

The relative sensitivity of the different sensors expected from the calibration data does not match precisely with the relative sensitivity measured by the transfer functions. For example, the transfer function from the ACO to the 324 Microflown RED particle velocity has an amplitude of about 3.6 judging from Figure 22. In contrast, the expected ratio of the voltages at 1 kHz would be

$$\frac{54.33\,{}^{mV}/_{Pa}}{15.4\,{}^{V}/_{m/s}} \cdot \frac{10^{-3}V}{mV} \cdot \frac{10^{9}\,{}^{nm}/_{s}}{{}^{m}/_{s}} \cdot \frac{20\mu Pa}{50\,{}^{nm}/_{s}} \cdot \frac{10^{-6}Pa}{\mu Pa} = 1.4 \ . \qquad (4.4)$$

The origin of this discrepancy is likely to include a number of factors including differences in the sensitivity of the individual sensors and their amplifiers, the specific impedance used to convert pressure and particle velocity, gain differences in the DAQ equipment channels, as well as—and probably most importantly—changes in sensitivity due to the sensor positions within the array. Regardless of the origin, the repeatability of the transfer functions suggest that they can be relied on for beamforming purposes and provide the best measure of determining the in situ pressure equivalent noise of the sensors.

THIS PAGE INTENTIONALLY LEFT BLANK

V. PRESSURE EQUIVALENT NOISE FLOOR MEASUREMENTS

To obtain the particle velocity sensor's noise floor, measurement of the sensor's noise signal was conducted in the Naval Postgraduate School's anechoic chamber to insulate against ambient noise. The signal conditioning boxes of the Microflown probes and the Data Acquisition Unit were grounded to the power supply reference ground to reduce stray electronic noise. In addition, for the period of measurement all electrical light sources and unused electronic fixtures in the chamber were turned off to reduce external electronic noise that could couple into the system readings. With these precautions in place, noise in the particle velocity channels should be limited to the thermal noise of the sensors themselves (which was the dominant source according to Microflown's analysis), electronic noise from the amplifiers and data acquisition equipment, and noise introduced by the transfer function measurements.

The pressure equivalent noise of the ACO microphone was computed first by collecting 256,000 samples (one minute) of its voltage output. The data was taken at a sampling frequency of 4267 Hz. The spectrum was computed with the *pwelch* command in MATLAB with a 1024 length Digital Fourier Transform length and a Hamming window. The raw voltage noise spectrum level obtained from the ACO is shown below. The data tip shows that near 1000 Hz, the spectrum level is $-127\,dB re 1V/\sqrt{Hz}$. The spectrum is quite flat after the low frequency noise has rolled off, so the measured voltage noise spectrum level can be converted to an octave band level with a center frequency of 1000 Hz and a dBA level. The correction between an A-weighted level and an octave band level is zero at a center frequency of 1000 Hz, and the bandwidth of an octave filter is 667 Hz with a center frequency of 1000 Hz [10]. Therefore, the voltage noise level is

$$NL = NSL + 10\log\Delta f = -127\,dB re 1V/\sqrt{Hz} + 10\log 667 = -99\,dB re 1V \ . \qquad (5.1)$$

This voltage noise level can be converted to an equivalent pressure noise level using the ACO sensitivity of 54.33 mV/Pa and then converting to the noise spectrum level $re\,20\mu Pa/\sqrt{Hz}$. $-99\,dB\,re\,1V$ corresponds to a voltage of

$$V = 1V \cdot 10^{-99/20} = 1.1 \times 10^{-5} V. \tag{5.2}$$

This voltage corresponds to a pressure of

$$\frac{1.1 \times 10^{-5} V}{54.33\,mV/Pa} \cdot \frac{10^3\,mV}{V} \cdot \frac{10^6\,\mu Pa}{Pa} = 200\,\mu Pa\ . \tag{5.3}$$

Finally, $200\,\mu Pa$ corresponds to a pressure noise level in the octave band of

$$NL = 20 \log \frac{200\,\mu Pa}{20\,\mu Pa} = 20\,dB\,re\,20\,\mu Pa\ . \tag{5.4}$$

This number is consistent with the pressure noise spectrum level of $-8\,dB\,re\,20\,\mu Pa/\sqrt{Hz}$ shown in Figure 26, since

$$NSL = NL - 10 \log \Delta f = 20dB - 10 \log 667 = -8dB\,re\,20\,\mu Pa/\sqrt{Hz}. \tag{5.5}$$

According to [12] the noise floor of the 7046 ACO microphone was measured by one of their other customers to be 10–12 dBA. We note that our measured value is about 10 dB higher than expected and corresponds to a factor of 10 in power or intensity or a factor of three in voltage or pressure.

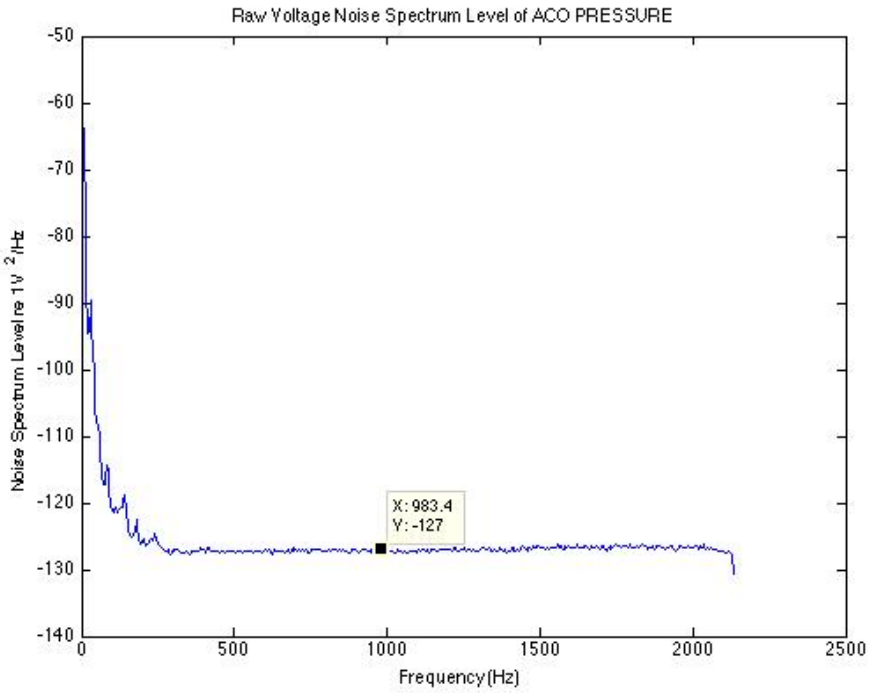

Figure 25. Raw voltage noise spectrum level of ACO microphone

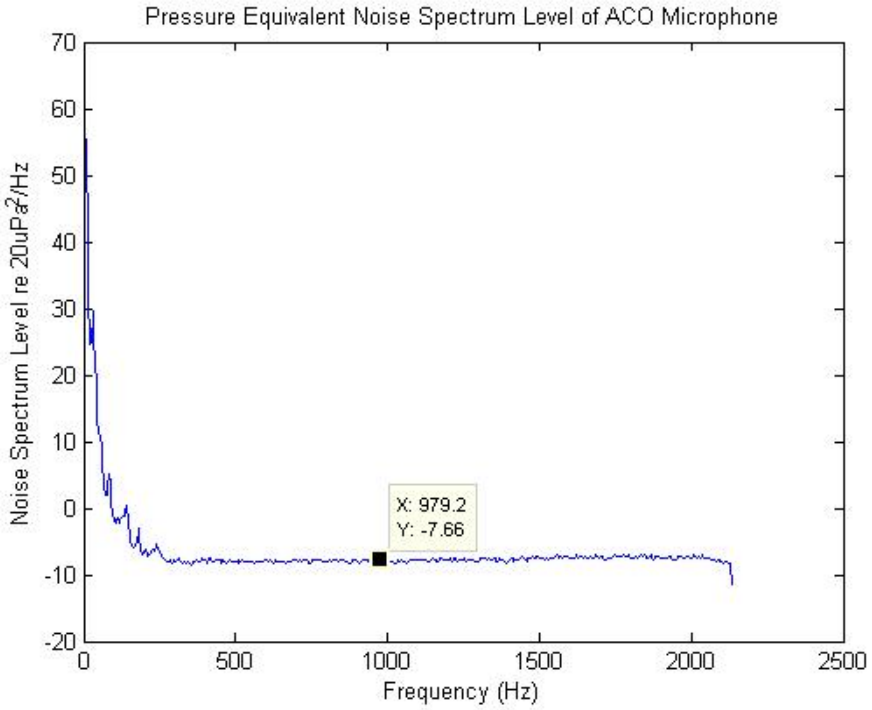

Figure 26. Noise spectrum level of ACO microphone

The raw voltage output of the Microflown pressure sensors measured under anechoic conditions are shown below.

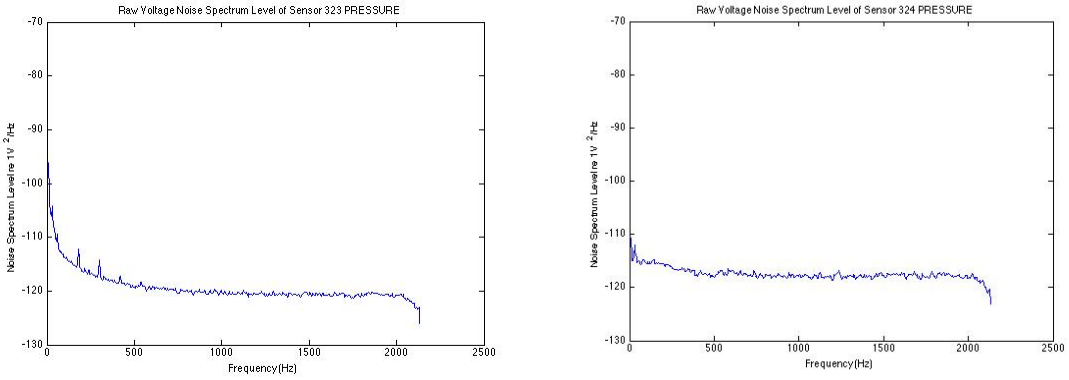

Figure 27. Raw voltage noise spectrum level of Microflown pressure sensors323 (left) and 324 (right)

Clearly, the 323 Microflown sensor was picking up considerable 60 Hz electromagnetic interference (EMI) and overtones. Previously, the 60 Hz interference had been considerably reduced with proper grounding. It is considered likely that the ground to the 323 signal conditioning box was loose, but there was no time to rectify the problem.

Converting the raw voltage of the 324 Microflown pressure sensor to pressure using its given sensitivity yields the noise spectrum level shown below. This agrees with the approximate calculated value. Starting with the voltage NSL of approximately $-118\,dBre^{1V}\!/\!\sqrt{Hz}$, the spectral density in terms of voltage is

$$-118\,dBre^{1V}\!/\!\sqrt{Hz} = 20\log\left(\frac{e/\sqrt{Hz}}{1V/\sqrt{Hz}}\right) \Rightarrow \qquad (5.6)$$

$$e/\sqrt{Hz} = 1V/\sqrt{Hz}\,10^{-118/20} = 1.3\times10^{-6}\,V/\sqrt{Hz}$$

Using the sensitivity of the 324 Microflown pressure sensor of $44.9\,mV\!/\!Pa$, this translates to a pressure noise spectral density of

$$\frac{1.3\times10^{-6}\ V/\sqrt{Hz}}{44.9\ mV/Pa}\cdot\frac{10^{3}\ mV}{V}\cdot\frac{10^{6}\ \mu Pa}{Pa}=29.0\ \mu Pa/\sqrt{Hz}. \tag{5.7}$$

The pressure noise spectrum level referenced to $20\,\mu Pa$ is then given by

$$NSL=20\log\left(\frac{29.0\,\mu Pa/\sqrt{Hz}}{20\,\mu Pa/\sqrt{Hz}}\right)=3\,dB\,re\ 20\,\mu Pa/\sqrt{Hz}\ . \tag{5.8}$$

The noise floor appears to be about 11 dB above the noise floor of the ACO microphone. This is not surprising considering its smaller size.

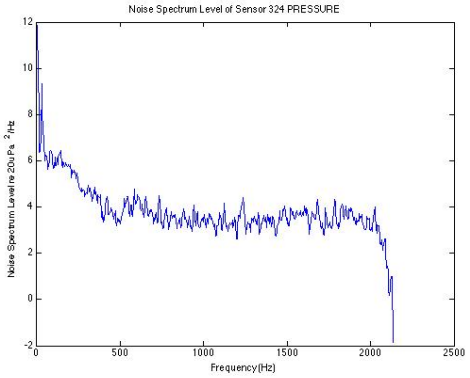

Figure 28. Pressure noise spectrum level of the 324 Microflown pressure sensor

Like the ACO microphone, the measured noise spectrum level of the Microflown microphone is higher than the value provided by the manufacturer [5]. Judging from the self-noise values shown in Figure 3, the measured value is approximately 14 dB higher. Although not explicitly indicated on the graph, the customary reference for in-air measurements of $20\,\mu Pa/\sqrt{Hz}$ is consistently applied in Microflown documents.

Before looking at the pressure equivalent noise spectrum level of the particle velocity channels, their raw voltage noise spectrum level was also computed. The figures below show the results for the BLUE sensors of both the 323 and 324 probes.

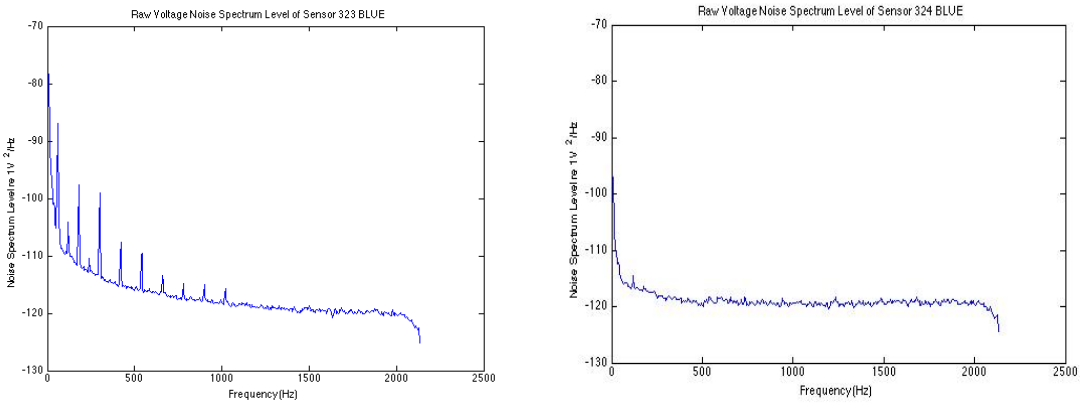

Figure 29. Raw voltage noise spectrum level of BLUE sensors323 (left)and 324 (right)

Clearly the 323 Microflown BLUE sensor suffers even more from the 60 Hz problem than the pressure sensor. The other particle velocity channels of the 323 Microflown showed similar results. Both spectra show a flattening noise floor at higher frequencies which is about 4 dB below the prediction in Equation 2.9.

To get the pressure equivalent noise of the particle velocity channels, the transfer function between the ACO microphone and the particle velocity sensor needs to be used. As given in the theory section, the "corrected" version of the particle velocity channel is given by

$$\hat{P}_{2b}(k) = \hat{F}_{P2}(k)\hat{H}_{2b}(k)\hat{X}_{2b}(k). \tag{5.9}$$

Using the voltage output of the particle velocity sensor in the absence of an acoustic signal, this quantity represents the pressure equivalent noise of the sensor. The spectrum of this noise was computed for all of the particle velocity sensors. Applying the transfer functions to the noise signals from the particle velocity sensors and expressing in terms of a noise spectrum level with the standard reference of $20\mu Pa/\sqrt{Hz}$ yields the spectrums shown below. For contrast, the pressure equivalent noise of the ACO microphone is shown on the same graph.

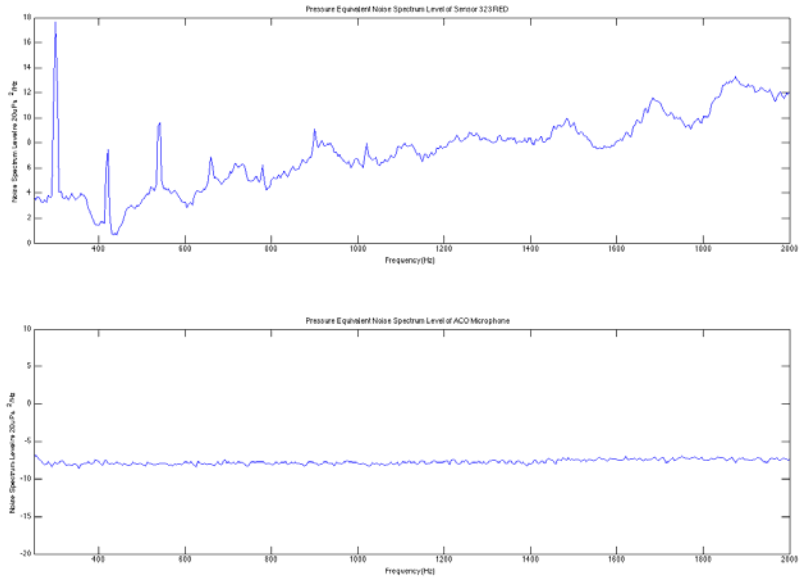

Figure 30. Pressure equivalent noise spectrum level of the 323 RED particle velocity sensor (above) as compared to the ACO microphone (below)

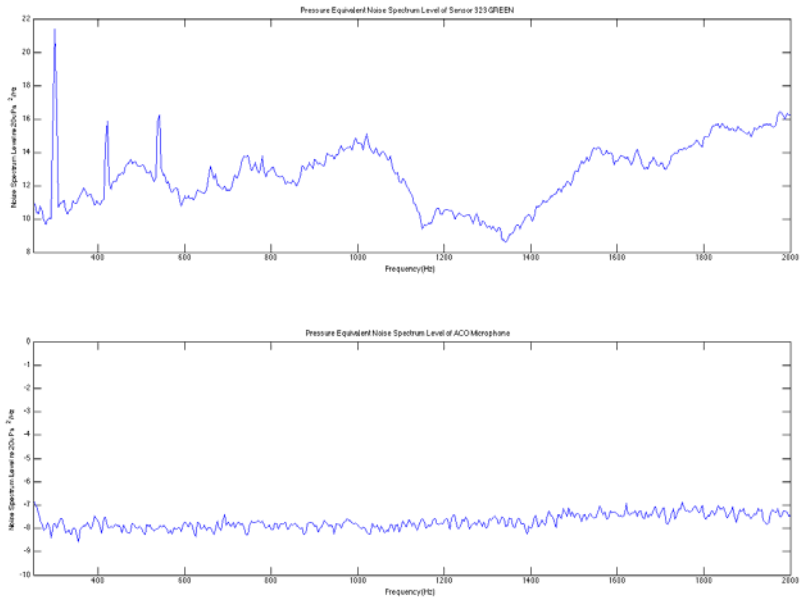

Figure 31. Pressure equivalent noise spectrum level of the 323 GREEN particle velocity sensor (above) as compared to the ACO microphone (below)

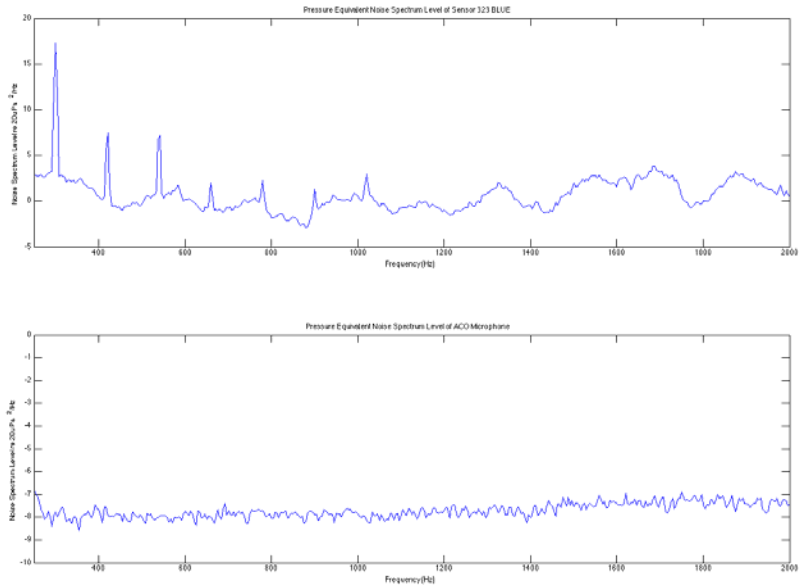

Figure 32. Pressure equivalent noise spectrum level of the 323 BLUE particle velocity sensor (above) as compared to the ACO microphone (below)

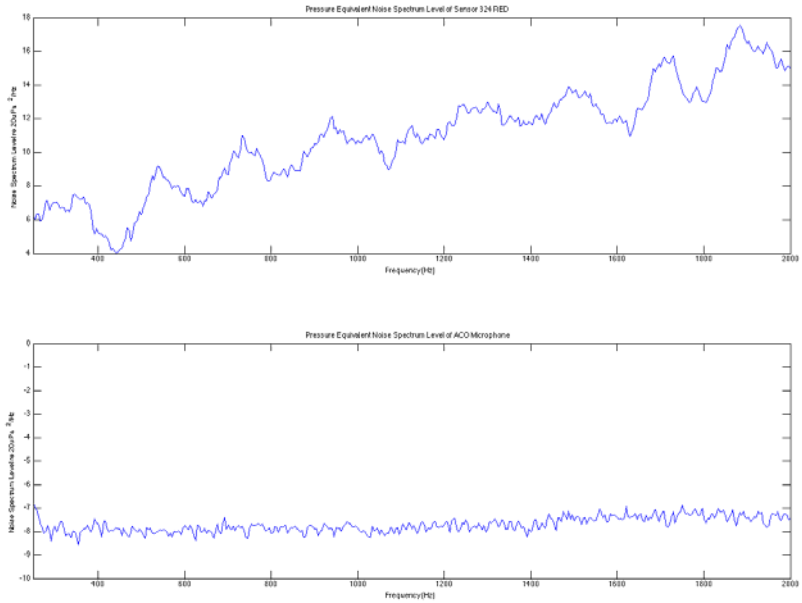

Figure 33. Pressure equivalent noise spectrum level of the 324 RED particle velocity sensor (above) as compared to the ACO microphone (below)

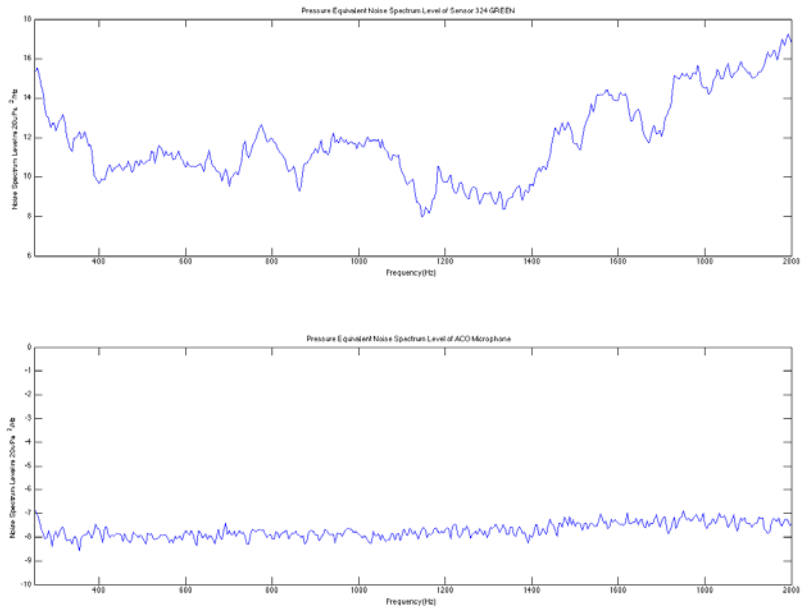

Figure 34. Pressure equivalent noise spectrum level of the 324 GREEN particle velocity sensor (above) as compared to the ACO microphone (below)

Figure 35. Pressure equivalent noise spectrum level of the 324 BLUE particle velocity sensor (above) as compared to the ACO microphone (below)

Clearly the noise in the ACO microphone is much flatter as a function of frequency than the noise of the Microflown particle velocity sensors. These variations are only partially predicted by theory. The voltage noise of the particle velocity sensor is constant across frequency when it is dominated by thermal noise; however, the sensitivity of the particle velocity sensors is frequency dependent. This is shown in Figure 36 below. All of the particle velocity calibration curves show similar behavior. The "uncorrected" mode was used for this work. Since the voltage is divided by the sensitivity to obtain pressure, the pressure equivalent noise spectrum level should decrease to a minimum at about 300–400 Hz and then increase gradually with frequency for a constant voltage noise spectrum level. The observed, rather erratic fluctuations are, therefore, artifacts of the changing sensitivity of the sensors in the holder as measured by the transfer functions.

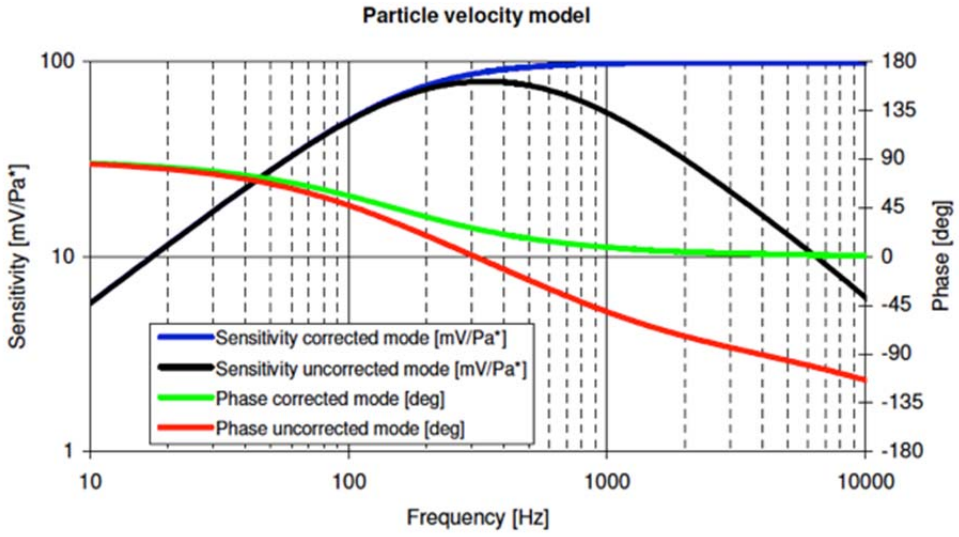

Figure 36. Sensitivity of 323 BLUE Microflown as a function of frequency(From [5])

Table 2 provides a summary of the results for the 324 Microflown (the one with the least amount of 60 Hz contamination). The measured pressure equivalent noise spectrum levels based on the transfer functions range from 9–15 dB larger than expected. These discrepancies correspond to voltages or pressures between about three and six times higher than expected. The fact that the raw voltage noise is quite flat across the spectrum of interest suggests that it is probably electronic. It is most likely introduced by

the NI 9234 DAQ modules which have an input range of +/–5V with a dynamic range of 102dB [9]. The standard deviation of the signals during the noise measurements were an order of magnitude of $10\mu V$. The published noise floor of the NI9234 modules when used with a 51.2 kS/s rate is $50\mu V$. Therefore, the performance of the hybrid array is more limited at low signal levels than anticipated by the sensor noise floors. The pressure equivalent noise spectrum levels obtained by converting the raw voltage noise spectrum levels by the manufacturers' calibration data are lower than the values obtained from the in situ transfer functions. This is the result of differences in the sensitivity of the sensors when positioned in the array.

Sensor	Measured raw voltage NSL	Pressure NSL (From manufacturer's calibration data)	Pressure NSL (From in situ transfer functions)	Expected pressure NSL
ACO	$-127\,dBre\,1V/\sqrt{Hz}$	$-8\,dBre\,20\mu Pa/\sqrt{Hz}$	$-8\,dBre\,20\mu Pa/\sqrt{Hz}$	$-18\,dBre\,20\mu Pa/\sqrt{Hz}$
324 pressure	$-118\,dBre\,1V/\sqrt{Hz}$	$3\,dBre\,20\mu Pa/\sqrt{Hz}$	$4\,dBre\,20\mu Pa/\sqrt{Hz}$	$-11\,dBre\,20\mu Pa/\sqrt{Hz}$
324 BLUE	$-119\,dBre\,1V/\sqrt{Hz}$	$3\,dBre\,20\mu Pa/\sqrt{Hz}$	$9\,dBre\,20\mu Pa/\sqrt{Hz}$	$0\,dBre\,20\mu Pa/\sqrt{Hz}$
324 GREEN	$-120\,dBre\,1V/\sqrt{Hz}$	$9\,dBre\,20\mu Pa/\sqrt{Hz}$	$12\,dBre\,20\mu Pa/\sqrt{Hz}$	$0\,dBre\,20\mu Pa/\sqrt{Hz}$
324 RED	$-120\,dBre\,1V/\sqrt{Hz}$	$2\,dBre\,20\mu Pa/\sqrt{Hz}$	$11\,dBre\,20\mu Pa/\sqrt{Hz}$	$0\,dBre\,20\mu Pa/\sqrt{Hz}$

Table 2. Summary of results. All values are at 1 kHz. dB levels +/– 1 dB

The final step of the measurements was to compare the performance of the particle velocity sensors with and without windscreens. One of the Microflown sensors was fitted with an ACO WS7 windscreen. Then both sensors in the array were placed in a windy location. An anemometer recorded the windspeed during the trial. Figure 37 below shows the results. The anemometer output was overlain on the graph to show the

qualitative windspeed. The windscreen clearly provides excellent protection from the broadband noise due to gusting wind. The tonal from a nearby ventilation fan is visible in both cases.

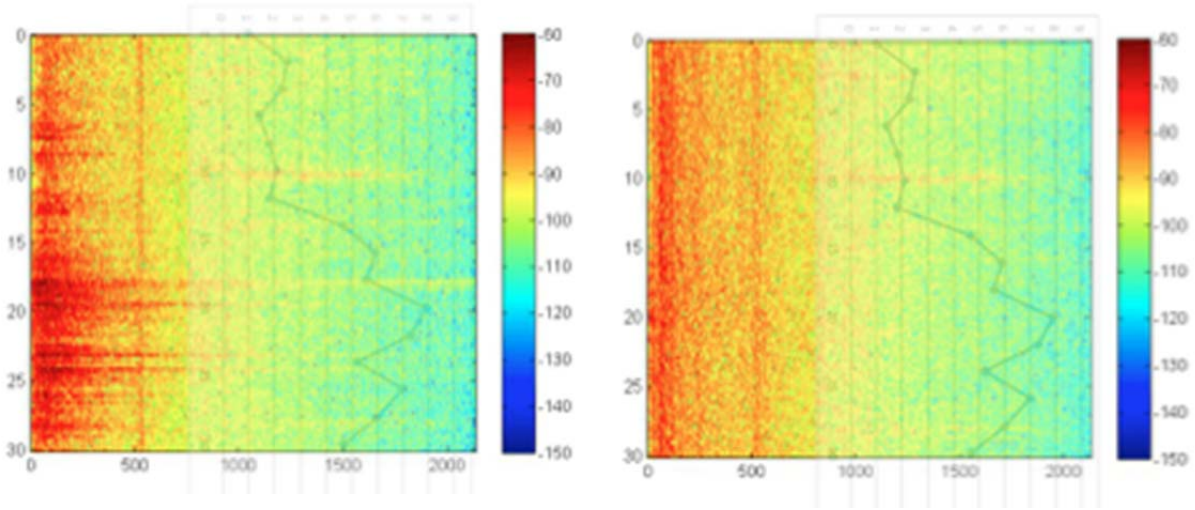

Figure 37. Graph of spectrum (horizontal axis) vs time (vertical axis) of signals collected on windy rooftop with windscreen off (left) and windscreen on (right)

VI. CONCLUSIONS AND RECOMMENDATIONS FOR FUTURE WORK

The pressure equivalent noise floor of the sensors in a hybrid array consisting of a conventional microphone and two Microflown vector sensors was successfully measured under anechoic conditions. The method used transfer functions established in situ between the Microflown sensors and the calibrated conventional microphone to ensure that any factors affecting the sensitivity of Microflown sensors relative to the conventional microphone were taken into account. The resulting pressure equivalent noise floors of both the conventional microphone and the Microflown sensors were 9–15 dB higher than expected. The increase was determined to result from the DAQ noise floor. In addition, a quick check on the performance of a WS7 windscreen was performed which showed a marked decrease in broadband noise due to gusting winds.

Future work might include an analysis of ambient acoustic noise under quiet conditions to determine whether the measured electronic noise floor is likely to be a limiting factor in field work. In addition, a study of the windscreen's performance with a wider variety of wind speeds would be helpful. Finally, the coherence of the noise between different channels should be checked to determine whether the theoretical array gain can be achieved.

THIS PAGE INTENTIONALLY LEFT BLANK

APPENDIX A. MATLAB CODE

```
% Program to read in Microflown data, compute transfer function between
% pressure sensor and velocity sensors, and then compute pressure
% equivalent noise levels
%

clear all
clc
close all

maxchan = 12;       %maximum number of data channels captured
numpass = 250;       %number of loop iterations in vi sampling routine
N = 1024;           %number of samples per channel per pass
M = numpass * N;    %total sample length per channel
Fs = 4267;          %sampling freq
NFFT = 2^10;
overlap = NFFT/2;
window = hanning(NFFT);

%%% CHANNEL DESIGNATIONS %%%
prs1 = 1; % sensor 324 pressure
blu1 = 2; % sensor 324 blu velocity
grn1 = 3; % sensor 324 grn velocity
red1 = 4; % sensor 324 red velocity
prsR = 5; % ACO pressure, chnl 6-8 not connected
prs2 = 9; % sensor 323 pressure
blu2 = 10; % sensor 323 blu velocity
grn2 = 11; % sensor 323 grn velocity
red2 = 12; % sensor 323 red velocity

Sref1 = prs2;   % Pressure Channel
Sref2 = blu2;   % Velocity Channel

plotsensor='Sensor 323';
plotref1='PRESSURE';
plotref2='BLUE';

datasets = 3;   %number of data sets for averaging
for ds=1:datasets  %cycle through number of data sets
%
%     if ds == 1
%         fid = fopen('Nov15_114700_323GREEN1.dat','r');     % bad
%     else if ds == 2
%             fid = fopen('Nov15_114834_323GREEN2.dat','r');
%         else if ds == 3
%                 fid = fopen('Nov15_114939_323GREEN3.dat','r');
%             end
%         end
%     end
%     if ds == 1
%         fid = fopen('14Nov160629_Ary_323_Scn_RedMRA_1.dat','r');
%     else if ds == 2
%             fid = fopen('14Nov160820_Ary_323_Scn_RedMRA_2.dat','r');
%         else if ds == 3
%                 fid =
fopen('14Nov160941_Ary_323_Scn_RedMRA_3.dat','r');
%             end
%         end
```

```
%     end
if ds == 1
        fid = fopen('14Nov154817_Ary_323_Scn_BlueMRA_1.dat','r');
elseif ds == 2
            fid = fopen('14Nov155220_Ary_323_Scn_BlueMRA_3.dat','r');
elseif ds == 3
                fid =
fopen('14Nov155220_Ary_323_Scn_BlueMRA_3.dat','r');
end
end
end
%     if ds == 1
%         fid = fopen('14Nov155751_Ary_324_Scn_RedMRA_1.dat','r');
%     else if ds == 2
%             fid = fopen('14Nov160031_Ary_324_Scn_RedMRA_2.dat','r');
%         else if ds == 3
%                 fid =
fopen('14Nov160158_Ary_324_Scn_RedMRA_3.dat','r');
%             end
%         end
%     end
%     if ds == 1
%         fid = fopen('Nov15_113456_324GREEN1.dat','r');
%     else if ds == 2
%             fid = fopen('Nov15_113614_324GREEN2.dat','r');
%         else if ds == 3
%                 fid = fopen('Nov15_113724_324GREEN3.dat','r');
%             end
%         end
%     end
%     if ds == 1
%         fid = fopen('14Nov153842_Ary_324_Scn_BlueMRA_1.dat','r');
%     else if ds == 2
%             fid = fopen('14Nov154050_Ary_324_Scn_BlueMRA_2.dat','r');
%         else if ds == 3
%                 fid =
fopen('14Nov154229_Ary_324_Scn_BlueMRA_3.dat','r');
%             end
%         end
%     end
frewind(fid)    %top of file
bindata = zeros(M,maxchan); %initialize matrix to allocate memory

for j = 1:numpass        %2400K datapoints = 96sec/chan
nextrow = (j-1)*N+1; %200K datapoint increments
bindata(nextrow:j*N,1:maxchan) = fread(fid, [N,maxchan] , 'float64',
'ieee-be');  %get 200K/chandatapoints
end
bindata = bindata';         %change to row data


    status = fclose('all'); % close all files


% Computation for Transfer Function for Sound Probe PRESSURE to velocity
channel
    gamma_p2v(:,ds) =
mscohere(bindata(Sref1,:),bindata(Sref2,:),window,overlap,NFFT,Fs);
    [P2V(:,ds),F] =
cpsd(bindata(Sref1,:),bindata(Sref2,:),window,overlap,NFFT,Fs);
    [V(:,ds),F] = pwelch(bindata(Sref2,:),window,overlap,NFFT,Fs);
    [P(:,ds),F] = pwelch(bindata(Sref1,:),window,overlap,NFFT,Fs);
```

```
    Hp2v(:,ds) = P2V(:,ds)./V(:,ds);   % Microflown PRESSURE TO Velocity

%Computation for ACO Reference to Microflown PRESSURE channel
gamma_pACO(:,ds) =
mscohere(bindata(prsR,:),bindata(Sref1,:),window,overlap,NFFT,Fs);
    [P2ACO(:,ds),F] =
cpsd(bindata(prsR,:),bindata(Sref1,:),window,overlap,NFFT,Fs);
    [P(:,ds),F] = pwelch(bindata(Sref1,:),window,overlap,NFFT,Fs);

    F2x(:,ds) = P2ACO(:,ds)./P(:,ds);   % ACO to PRESSURE

end

% PLOT VELOCITY ELEMENT to PRESSURE Transfer Function
    figure(1)

    subplot(3,1,1)
    hold on
    plot(F,gamma_p2v(:,1),'b')
    plot(F,gamma_p2v(:,2),'g')
    plot(F,gamma_p2v(:,3),'r')
ylabel('Coherence')
    title(['Coherence - ',plotsensor,': ',plotref1,' to ',plotref2, '
Velocity'])
    axis([0 2000 0 1.1])

    subplot(3,1,2)
    hold on
    plot(F,abs(Hp2v(:,1)),'b')
    plot(F,abs(Hp2v(:,2)),'g')
    plot(F,abs(Hp2v(:,3)),'r')
ylabel('Transfer Function Amplitude')
    title(['Amplitude of Transfer Function - ',plotsensor,':
',plotref1,' to ',plotref2, ' Velocity'])
    axis([0 2000 0 15])

    subplot(3,1,3)
    hold on
    plot(F, rad2deg(angle(Hp2v(:,1))),'b')
    plot(F, rad2deg(angle(Hp2v(:,2))),'g')
    plot(F, rad2deg(angle(Hp2v(:,3))),'r')
    title(['Phase Difference - ',plotsensor,': ',plotref1,' to
',plotref2, ' Velocity'])
ylabel('Phase Difference (deg)')
xlabel('Frequency (Hz)')
    axis([0 2000 -180 180])

    figure(2)

    subplot(3,1,1)
    hold on
    gamma_p2v=sum(gamma_p2v,2)/3;
    plot(F,gamma_p2v,'b')
ylabel('Coherence')
    title(['AVERAGED Coherence - ',plotsensor,': ',plotref1,' to
',plotref2, ' Velocity'])
    axis([0 2000 0 1])

    subplot(3,1,2)
    hold on
    Hp2v = sum(Hp2v,2)/3;
```

```
    plot(F,abs(Hp2v),'b')
ylabel('Transfer Function Amplitude')
    title(['AVERAGED Amplitude of Transfer Function - ',plotsensor,':
',plotref1,' to ',plotref2, ' Velocity'])
    axis([0 2000 0 10])

    subplot(3,1,3)
    hold on
    plot(F, rad2deg(angle(Hp2v)),'b')
    title(['Phase Difference - ',plotsensor,': ',plotref1,' to
',plotref2, ' Velocity'])
ylabel('AVERAGED Phase Difference (deg)')
xlabel('Frequency (Hz)')
    axis([0 2000 -180 180])

% PLOT PRESSURE to ACO Transfer Function
    figure(3)

    subplot(3,1,1)
    hold on
    plot(F,gamma_pACO(:,1),'b')
    plot(F,gamma_pACO(:,2),'g')
    plot(F,gamma_pACO(:,3),'r')
ylabel('Coherence')
    title(['Coherence - ',plotsensor,': ACO Microphone to ' ,plotref1])
    axis([0 2000 0 1])

    subplot(3,1,2)
    hold on
    plot(F,abs(F2x(:,1)),'b')
    plot(F,abs(F2x(:,2)),'g')
    plot(F,abs(F2x(:,3)),'r')
ylabel('Transfer Function Amplitude')
    title(['Amplitude of Transfer Function - ',plotsensor,': ACO
Microphone to ' ,plotref1])
    axis([0 2000 0 15])

    subplot(3,1,3)
    hold on
    plot(F, rad2deg(angle(F2x(:,1))),'b')
    plot(F, rad2deg(angle(F2x(:,2))),'g')
    plot(F, rad2deg(angle(F2x(:,3))),'r')
    title(['Phase Difference - ',plotsensor,': ACO Microphone to '
,plotref1])
ylabel('Phase Difference (deg)')
xlabel('Frequency (Hz)')
    axis([0 2000 -180 180])

    figure(4)

    subplot(3,1,1)
    hold on
gamma_pACO=sum(gamma_pACO,2)/3;
    plot(F,gamma_pACO,'k')
ylabel('Coherence')
    title(['AVERAGED Coherence - ',plotsensor,': ACO Microphone to '
,plotref1])
    axis([0 2000 0 1])

    subplot(3,1,2)
    hold on
```

```
    F2x = sum(F2x,2)/3;
    plot(F,abs(F2x),'k')
ylabel('Transfer Function Amplitude')
    title(['AVERAGED Amplitude of Transfer Function - ',plotsensor,':
ACO Microphone to ' ,plotref1])
    axis([0 2000 0 15])

    subplot(3,1,3)
    hold on
    plot(F, rad2deg(angle(F2x)),'k')
    title(['AVERAGED Phase Difference - ',plotsensor,': ACO Microphone
to ' ,plotref1])
ylabel('Phase Difference (deg)')
xlabel('Frequency (Hz)')
    axis([0 2000 -180 180])


    figure(5)

    subplot(2,1,1)
    FH=Hp2v.*F2x;  %transfer function to correct velocity to ACO
pressure direct
    plot(F,abs(FH),'k')
ylabel('Transfer Function Amplitude')
    title(['Amplitude of Transfer Function - ',plotsensor,': ACO
Microphone to ',plotref2,' Velocity'])
%axis([0 2000 0 100])

    subplot(2,1,2)
    plot(F,rad2deg(angle(FH)),'k')
ylabel('Phase Difference (deg)')
xlabel('Frequency (Hz)')
%axis([0 2000 -180 180])

    fid = fopen('14Nov164432_NFLoor1.dat','r');
frewind(fid)    %top of file
bindata = zeros(M,maxchan); %initialize matrix to allocate memory
    m=0.05433;  %aco sensitivity

for j = 1:numpass
nextrow = (j-1)*N+1;
bindata(nextrow:j*N,1:maxchan) = fread(fid, [N,maxchan] , 'float64',
'ieee-be');
end
bindata = bindata';          %change to row data
    status = fclose('all'); % close all files



noise_signal = bindata(Sref2,:);
noise_signal = noise_signal - mean(noise_signal);
penf=pwelch(noise_signal,window,overlap,NFFT,Fs);
raw_noise = penf;
raw_noise = 10*log10(raw_noise);
penf=penf.*(FH.*conj(FH))/m^2*1E12/400;  %pressure equivalent noise
floor computation re 20uPa
penf = 10*log10(penf);

 figure(6)

 plot(F,raw_noise)
```

```
xlabel('Frequency (Hz)')
ylabel('Noise Spectrum Level re 1V^2/Hz')
 title(['Raw Voltage Noise Spectrum Level of ',plotsensor,' ' plotref2])


ACO = bindata(prsR,:);
ACO = ACO - mean(ACO);
[PACO, F] = pwelch(ACO,window,overlap,NFFT,Fs);
PACO = PACO/m^2;  % ACO corrected to Pa
PACO = PACO*1E12/400;  % ACO signal in 20uPa
PACO = 10*log10(PACO);

 figure(7)

 subplot(2,1,1)
 plot(F,penf)
xlabel('Frequency (Hz)')
ylabel('Noise Spectrum Level re 20uPa^2/Hz')
 title(['Pressure Equivalent Noise Spectrum Level of ',plotsensor,' '
plotref2])

 subplot(2,1,2)
 plot(F,PACO)
xlabel('Frequency (Hz)')
ylabel('Noise Spectrum Level re 20uPa^2/Hz')
 title('Pressure Equivalent Noise Spectrum Level of ACO Microphone')
```

APPENDIX B. CALIBRATION REPORT OF MICROFLOWN 324 ULTIMATE SOUND PROBE [5]

Microflwn Technologies
Charting sound fields

Calibration Report

Microflown kit:	324
Signal conditioner	E0901-24
USP probe regular	UT0901-24

Calibrated with GRAS 40AC reference pressure microphone

Checks performed:	
☐	Audio test
☐	Precalibration test
☐	Signal conditioner adjusted
☐	Mechanical check
☐	Full calibration
☐	Final check

Calibration Date : 19-2-2009

Calibrator	Supervisor
V.A. Hendriks	R.C. Platenkamp

Microflown Technologies
PO Box 300
6900 AH Zevenaar
The Netherlands
T: +31 316 581 490
F: +31 316 581 491
E: info@microflown.com

Additional information

What does high and low gain mean?

The high/low gain and equaliser switches only affect the particle velocity output of the signal conditioner. The pressure output of the signal conditioner is unaffected!

When the signal conditioner switch is in lower position the low gain option is selected. Then particle velocity output of the signal conditioner (in Volts) is the same as the output of the Microflown (in Volts).

When the signal conditioner switch is in upper position the high gain option is selected. The particle velocity output of the signal conditiner is then amplified with 42 dB.

What does the equaliser option mean?

The equaliser option equalises the amplitude and phase response of the particle velocity signal.

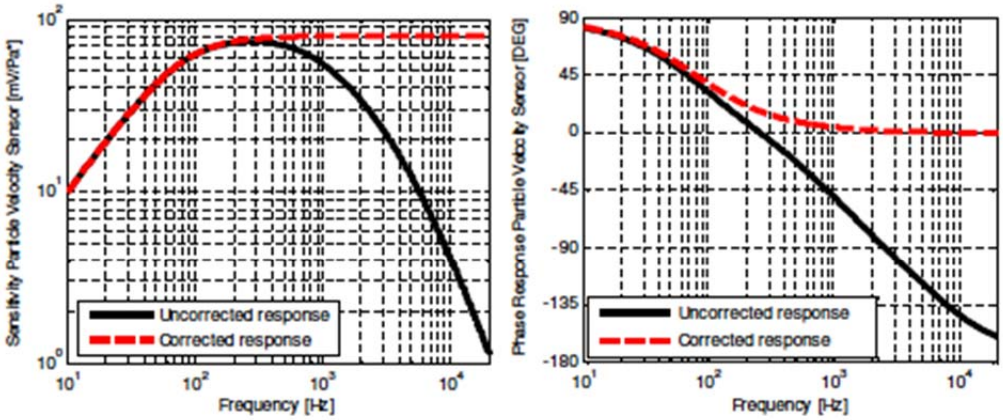

The left figure shows the amplitude response in uncorrected and corrected mode, the right figure shows the phase response.

Selfnoise

Typical selfnoise boundries of the pressure and the particle velocity sensor:

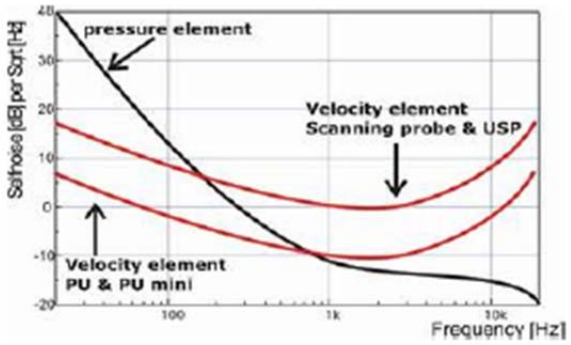

Model sound pressure microphone

Kit : 324	UT0901-24	19 February 2009

The sensitivity of the pressure sensor (independent of high/low gain or corrected/ uncorrected mode):

$$S_p\,[mV/Pa] = S_p\,@1kHz \frac{\sqrt{1+\frac{f^2}{f_{c3p}^2}}}{\sqrt{1+\frac{f_{c1p}^2}{f^2}}\sqrt{1+\frac{f_{c2p}^2}{f^2}}}$$

Parameters pressure equations		
Sensitivity:		
S_p @1kHz=	44,9	[mV/Pa]
Sensitivity cornerfrequencies		
fc1p=	69	[Hz]
fc2p=	15	[Hz]
fc3p=	5772	[Hz]
Phase cornerfrequencies		
C1p=	65	[Hz]
C2p=	14	[Hz]
C3p=	18828	[Hz]

The phase of the pressure sensor (independent of high/low gain or corrected/uncorrected mode):

$$\varphi_p\,[\mathrm{deg}] = \arctan\frac{C_{1p}}{f} + \arctan\frac{C_{2p}}{f} + \arctan\frac{f}{C_{3p}}$$

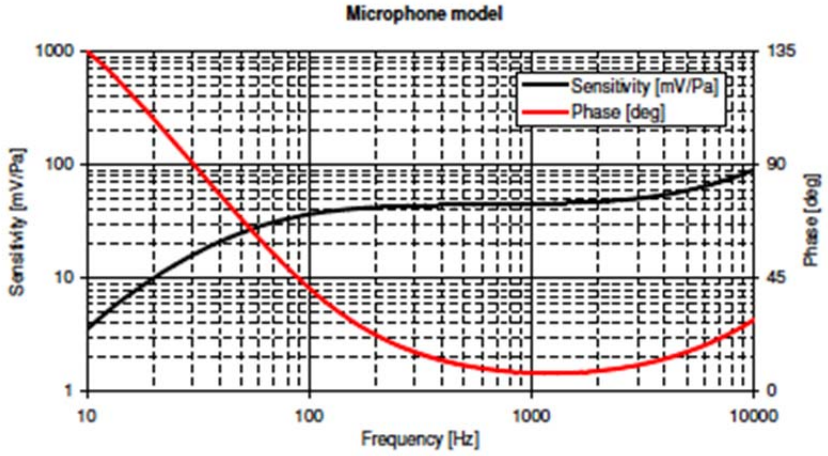

Model velocity sensor (blue element)

Kit : 324	UT0901-24	19 February 2009

Particle velocity sensitivity in uncorrected mode:

$$S_u[mV/Pa^*] = \frac{S_u @ 250Hz}{\sqrt{1+\frac{f_{c1u}^2}{f^2}}\sqrt{1+\frac{f^2}{f_{c2u}^2}}\sqrt{1+\frac{f^2}{f_{c3u}^2}}}$$

Particle velocity phase in uncorrected mode:

$$\varphi_u[\deg] = \arctan\frac{C_{1u}}{f} - \arctan\frac{f}{C_{2u}} - \arctan\frac{f}{C_{3u}}$$

Particle velocity sensitivity in corrected mode:

$$S_u[mV/Pa^*] = \frac{S_u @ 250Hz}{\sqrt{1+\frac{f_{c1u}^2}{f^2}}}$$

Particle velocity phase in corrected mode:

$$\varphi_u[\deg] = \arctan\frac{C_{1u}}{f}$$

Parameters velocity equations		
Sensitivity in high gain:		
Su @250Hz=	60,3	[mV/Pa*]
Su @250Hz=	24,8	[V/(m/s)]
Sensitivity in low gain:		
Su @250Hz=	0,5	[mV/Pa*]
Su @250Hz=	0,2	[V/(m/s)]
Sensitivity cornerfrequencies		
fc1u=	110	[Hz]
fc2u=	840	[Hz]
fc3u=	20356	[Hz]
Phase cornerfrequencies		
C1u=	117	[Hz]
C2u=	751	[Hz]
C3u=	18279	[Hz]

Particle velocity model

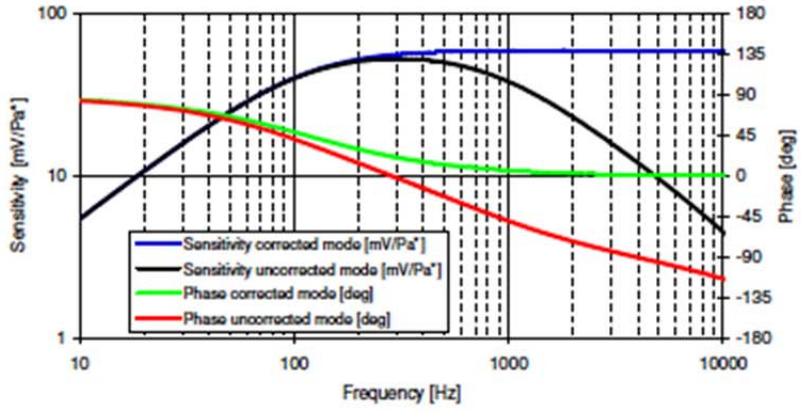

Model velocity sensor (blue element)

Kit : 324	UT0901-24	19 February 2009

Pu phase in uncorrected mode (independent of high/low gain):

$$\varphi_{pu}[\deg] = \arctan\frac{C_{1x}}{f} - \arctan\frac{f}{C_{2x}} - \arctan\frac{f}{C_{3x}} - \arctan\frac{C_{1y}}{f} - \arctan\frac{C_{2y}}{f} - \arctan\frac{f}{C_{3y}}$$

Pu phase in corrected mode (independent of high/low gain):

$$\varphi_{pu}[\deg] = \arctan\frac{C_{1x}}{f} - \arctan\frac{C_{1y}}{f} - \arctan\frac{C_{2y}}{f} - \arctan\frac{f}{C_{3y}}$$

Parameters pu phase equations		
Pressure cornerfrequencies		
C1p=	65	[Hz]
C2p=	14	[Hz]
C3p=	18828	[Hz]
Velocity cornerfrequencies		
C1u=	117	[Hz]
C2u=	751	[Hz]
C3u=	18279	[Hz]

Model velocity sensor (green element)

Kit : 324	UT0901-24	19 February 2009

Particle velocity sensitivity in uncorrected mode:

$$S_u[mV/Pa^*] = \frac{S_u @ 250Hz}{\sqrt{1+\frac{f_{c1u}^2}{f^2}}\sqrt{1+\frac{f^2}{f_{c2u}^2}}\sqrt{1+\frac{f^2}{f_{c3u}^2}}}$$

Particle velocity phase in uncorrected mode:

$$\varphi_u[\deg] = \arctan\frac{C_{1u}}{f} - \arctan\frac{f}{C_{2u}} - \arctan\frac{f}{C_{3u}}$$

Particle velocity sensitivity in corrected mode:

$$S_u[mV/Pa^*] = \frac{S_u @ 250Hz}{\sqrt{1+\frac{f_{c1u}^2}{f^2}}}$$

Particle velocity phase in corrected mode:

$$\varphi_u[\deg] = \arctan\frac{C_{1u}}{f}$$

Parameters velocity equations		
Sensitivity in high gain:		
Su @250Hz=	30,2	[mV/Pa*]
Su @250Hz=	12,4	[V/(m/s)]
Sensitivity in low gain:		
Su @250Hz=	0,2	[mV/Pa*]
Su @250Hz=	0,1	[V/(m/s)]
Sensitivity cornerfrequencies		
fc1u=	117	[Hz]
fc2u=	649	[Hz]
fc3u=	Inf	[Hz]
Phase cornerfrequencies		
C1u=	113	[Hz]
C2u=	751	[Hz]
C3u=	7531	[Hz]

Particle velocity model

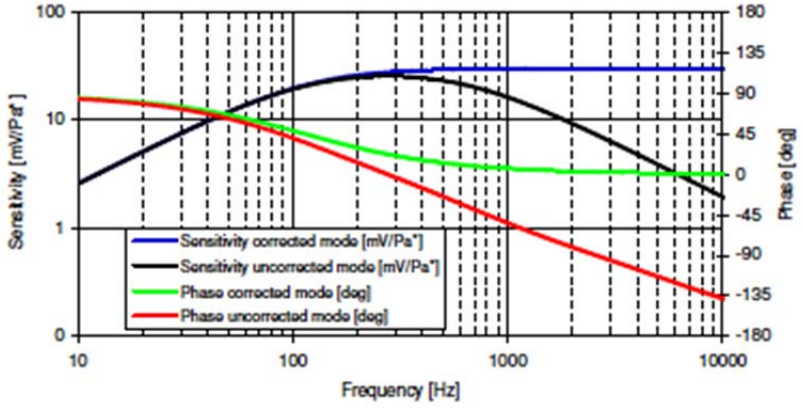

Model phase pressure - velocity (green element)

Kit : 324	UT0901-24	19 February 2009

Pu phase in uncorrected mode (independent of high/low gain):

$$\varphi_{pu}[\deg] = \arctan\frac{C_{1x}}{f} - \arctan\frac{f}{C_{2x}} - \arctan\frac{f}{C_{3x}} - \arctan\frac{C_{1y}}{f} - \arctan\frac{C_{2y}}{f} - \arctan\frac{f}{C_{3y}}$$

Pu phase in corrected mode (independent of high/low gain):

$$\varphi_{pu}[\deg] = \arctan\frac{C_{1x}}{f} - \arctan\frac{C_{1y}}{f} - \arctan\frac{C_{2y}}{f} - \arctan\frac{f}{C_{3y}}$$

Parameters pu phase equations		
Pressure cornerfrequencies		
C1p=	65	[Hz]
C2p=	14	[Hz]
C3p=	18828	[Hz]
Velocity cornerfrequencies		
C1u=	113	[Hz]
C2u=	751	[Hz]
C3u=	7531	[Hz]

Model velocity sensor (red element)

Kit : 324	UT0901-24	19 February 2009

Particle velocity sensitivity in uncorrected mode:

$$S_u[mV/Pa^*] = \frac{S_u @ 250Hz}{\sqrt{1+\frac{f_{c1u}^2}{f^2}}\sqrt{1+\frac{f^2}{f_{c2u}^2}}\sqrt{1+\frac{f^2}{f_{c3u}^2}}}$$

Particle velocity phase in uncorrected mode:

$$\varphi_u[\deg] = \arctan\frac{C_{1u}}{f} - \arctan\frac{f}{C_{2u}} - \arctan\frac{f}{C_{3u}}$$

Particle velocity sensitivity in corrected mode:

$$S_u[mV/Pa^*] = \frac{S_u @ 250Hz}{\sqrt{1+\frac{f_{c1u}^2}{f^2}}}$$

Particle velocity phase in corrected mode:

$$\varphi_u[\deg] = \arctan\frac{C_{1u}}{f}$$

Parameters velocity equations		
Sensitivity in high gain:		
Su @250Hz=	61,5	[mV/Pa*]
Su @250Hz=	25,3	[V/(m/s)]
Sensitivity in low gain:		
Su @250Hz=	0,5	[mV/Pa*]
Su @250Hz=	0,2	[V/(m/s)]
Sensitivity cornerfrequencies		
fc1u=	113	[Hz]
fc2u=	776	[Hz]
fc3u=	Inf	[Hz]
Phase cornerfrequencies		
C1u=	124	[Hz]
C2u=	648	[Hz]
C3u=	15768	[Hz]

Particle velocity model

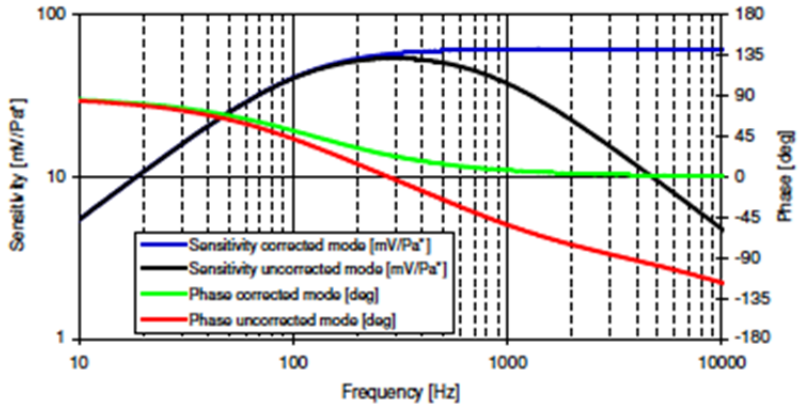

Model phase pressure - velocity (red element)

Kit : 324	UT0901-24	19 February 2009

Pu phase in uncorrected mode (independent of high/low gain):

$$\varphi_{pu}[\deg] = \arctan\frac{C_{1x}}{f} - \arctan\frac{f}{C_{2x}} - \arctan\frac{f}{C_{3x}} - \arctan\frac{C_{1y}}{f} - \arctan\frac{C_{2y}}{f} - \arctan\frac{f}{C_{3y}}$$

Pu phase in corrected mode (independent of high/low gain):

$$\varphi_{pu}[\deg] = \arctan\frac{C_{1x}}{f} - \arctan\frac{C_{1y}}{f} - \arctan\frac{C_{2y}}{f} - \arctan\frac{f}{C_{3y}}$$

Parameters pu phase equations		
Pressure cornerfrequencies		
C1p=	65	[Hz]
C2p=	14	[Hz]
C3p=	18828	[Hz]
Velocity cornerfrequencies		
C1u=	124	[Hz]
C2u=	648	[Hz]
C3u=	15768	[Hz]

THIS PAGE INTENTIONALLY LEFT BLANK

APPENDIX C. ACO MICROPHONE SPECIFICATIONS

MICROPHONE CALIBRATION DATA [13]

CONDENSER MICROPHONE
FREQUENCY RESPONSE

CARTRIDGE TYPE 7046

SERIAL No. 36930

ACO

dB

-25.3 dB re. 1 V per pascal or 54.33 mV per pascal

Open Circuit Correction Factor:

K_0 = ... dB

Cartridge Capacitance:

C = 20.5 pF

Leakage Resistance tested at 52%relative humidity
>$10^{10}\Omega$

Conditions of Test:

Frequency: 250 Hz

Polarization voltage:200 V

Ambient Static Pressure: 1023 hPa

Relative Humidity: 40 %

Temperature: 22 °C

MAR 2 4 2005

Date: ..... Signature: .....

1 pascal = 1 N/m^2 = 10 μbar

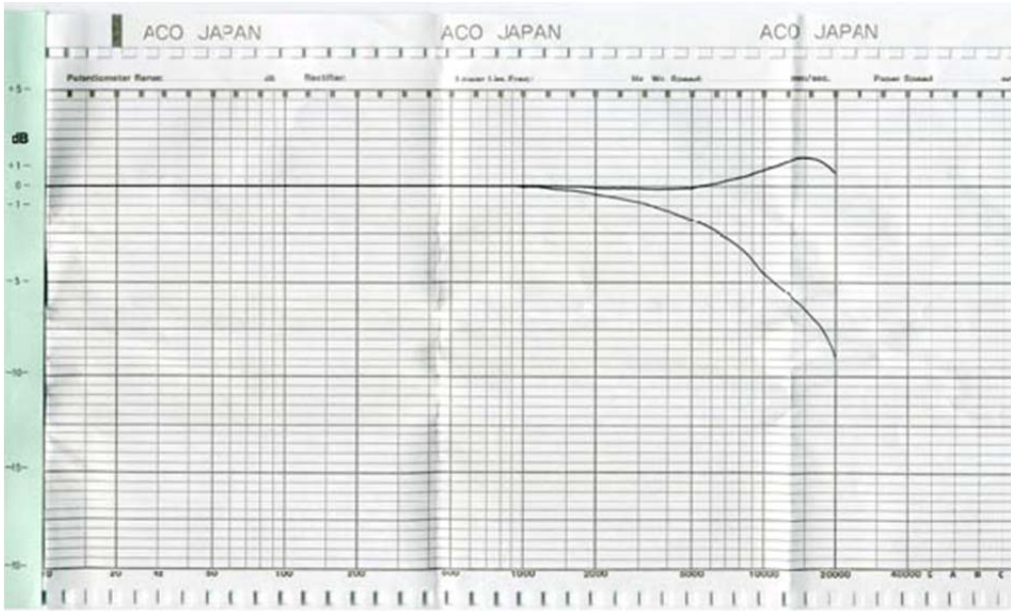

ACO MICROPHONE PRE-AMPLIFIER SPECIFICATIONS [14]

4012 Family

Specifications: Typical

- 28 Vdc, 22 pF (DM2-22 Dummy Mic) Terminated
- Frequency Response:
  <2 Hz to >200 kHz +/- 0.5 dB,
  0.5 Hz to >> 200 kHz +/- 2 dB
- Insertion Loss: <<0.25 dB @ 1 kHz
- Noise:
  "A" Weighted - <1.2 uV typ.
  Linear 20 to 20 kHz - 3 uV
- Input Impedance: >50 G//0.1 pF
- Output Voltage: >7 Vrms @28 Vdc Typical
  >15 Vrms @50 Vdc
- Power Requirements:
  28 Vdc @ <1 mA (HP option <2 mA)
  50 Vdc @ <2 mA (HP option <4 mA)

Models :

- 4012 w/CA4012 Cable (5 pin XLR)
- 4012L7 w/CA4012L7 Cable (7 pin Lemo)
- 40L12 - Lemo 1B 7 Pin Male Connector on base
- 40X12 - XLR 5 pin Male Connector on Base
- "HP" Version - Higher Operating Current Option
- Standard Cable Length 2 Meters
- 4016 - 4012 Preamp and AD0016 1/4" to 1/2" Adaptor
- 4022 - 4012 Preamp and AD0122 1" to 1/2" Adaptor

APPENDIX D. NI9234 TECHNICAL SPECIFICATIONS, EXCERPT [9]

Alias-free bandwidth ..... $0.45 \cdot f_s$

Oversample rate ..... $64 \cdot f_s$

Crosstalk (1 kHz) ..... –110 dB

CMRR ($f_{in} \leq 1$ kHz)

Minimum ..... 40 dB

Typical ..... 47 dB

SFDR (f_{in} = 1 kHz, –60 dBFS) ..... 120 dB

Idle channel noise and noise density

Idle Channel	51.2 kS/s	25.6 kS/s	2.048 kS/s
Noise	97 dBFS	99 dBFS	103 dBFS
	50 μV_{rms}	40 μV_{rms}	25 μV_{rms}
Noise density	310 nV/√Hz	350 nV/√Hz	780 nV/√Hz

Input impedance

Differential ..... 305 kΩ

AI– (shield) to chassis ground.... 50 Ω

THIS PAGE INTENTIONALLY LEFT BLANK

APPENDIX E. ACO WS-7 WINDSCREEN ATTENUATION [15]

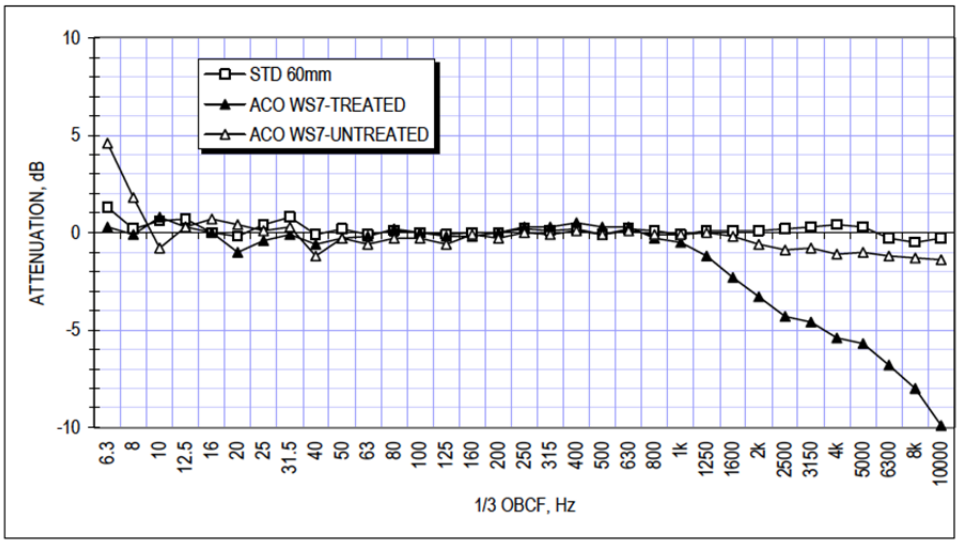

Graphic courtesy of Hessler Associates, Inc.

Figure 2: *Windscreen attenuation fitted with manufactureres standard 60mm unit and ACO pacific model WS7 units*

THIS PAGE INTENTIONALLY LEFT BLANK

LIST OF REFERENCES

[1] J. V. Caulk, "Experimental and theoretical performance of a particle velocity vector sensor in a hybrid acoustic beamformer," M.S. thesis, Eng. Acoust. Academic Committee, Naval Postgraduate School, Monterey, CA, 2009.

[2] H. E. de Bree, *The Microflown: a true particle velocity microphone; sound intensity application*, 1998 [Online]. Available: http://www.microflown.com/files/media/library/Publications/Miscellaneaous/nag_1998-overzichtspublicatie_nag.pdf

[3] H. E. de Bree and M. Elwenspoek, "Improving the signal to noise ratio of resistive sensors" [Online], MESA Research Inst., Univ. of Twente, Enschede, The Netherlands, 1999, Available: http://www.microflown.com/files/media/library/Publications/Miscellaneaous/mme_99.pdf

[4] D. R. Yntema et al., "A three dimensional Microflown," in *Proc. of the 19th IEEE Int. Conf. on Micro Electro Mech. Syst.*, Istanbul, Turkey, 2006, pp. 654–657.

[5] Microflown Technologies, Calibration Report, Microflown kit: 323, 2009.

[6] H. E. de Bree et al., "Three-dimensional sound intensity measurements using Microflown particle velocity sensors," in *Proc. of the 12th IEEE Int. Conf. on Micro Electro Mech. Syst.*, Orlando, FL, 1999, pp. 124–129.

[7] H. E. de Bree, *The Microflown E-Book*, 2009 [Online]. Available: http://www.microflown.com/library/books/the-microflown-e-book.html

[8] B. A. Cray and A. H. Nuttall, "Directivity factors for linear arrays of velocity sensors," *J. Acoust. Soc. Amer.*, vol. 110, no. 1, pp. 324–331, Jul. 2001.

[9] National Instruments Corp., "NI 9234 Operating Instructions and Specifications," Aug. 2008.

[10] L. E. Kinsler et al., *Fundamentals of Acoustics*, 5th ed. New York, NY: Wiley & Sons, 2000.

[11] P. Stoica and R. Moses, *Introduction to Spectral Analysis*. Upper Saddle River, NJ: Prentice Hall, 2005.

[12] N. Lewis, private communication, 1997.

[13] ACO Pacific, Inc. "Condenser Microphone Frequency Response, Serial No 36930."

[14] ACO Pacific, Inc. *ACOtron Preamp Specifications – 4012 Family* [Online]. Available: http://www.acopacific.com/acotrndt.html#4012

[15] ACO Pacific, Inc., "ACO Technical Bulletin Number 04809-1: Windscreens for improved low frequency noise (LFN) measurements."

INITIAL DISTRIBUTION LIST

1. Defense Technical Information Center
   Ft. Belvoir, Virginia

2. Dudley Knox Library
   Naval Postgraduate School
   Monterey, California

3. Professor Andres Larraza
   Code PH/La
   Naval Postgraduate School
   Monterey, California

4. Professor Daphne Kapolka
   Code PH/Kd
   Naval Postgraduate School
   Monterey, California

5. Professor Kevin B. Smith
   Code PH/Sk
   Naval Postgraduate School
   Monterey, California

6. Professor Yeo Tat Soon
   Director, Temasek Defence Science Institute
   National University of Singapore
   Singapore

7. Tan Lai Poh (Ms)
   Assistant Manager, Temasek Defence Science Institute
   National University of Singapore
   Singapore

8. Kok Chuen Wah
   Ministry of Defence
   Singapore